# The Rhodes Journal of Biological Sciences

## Volume XVIII Spring 2001

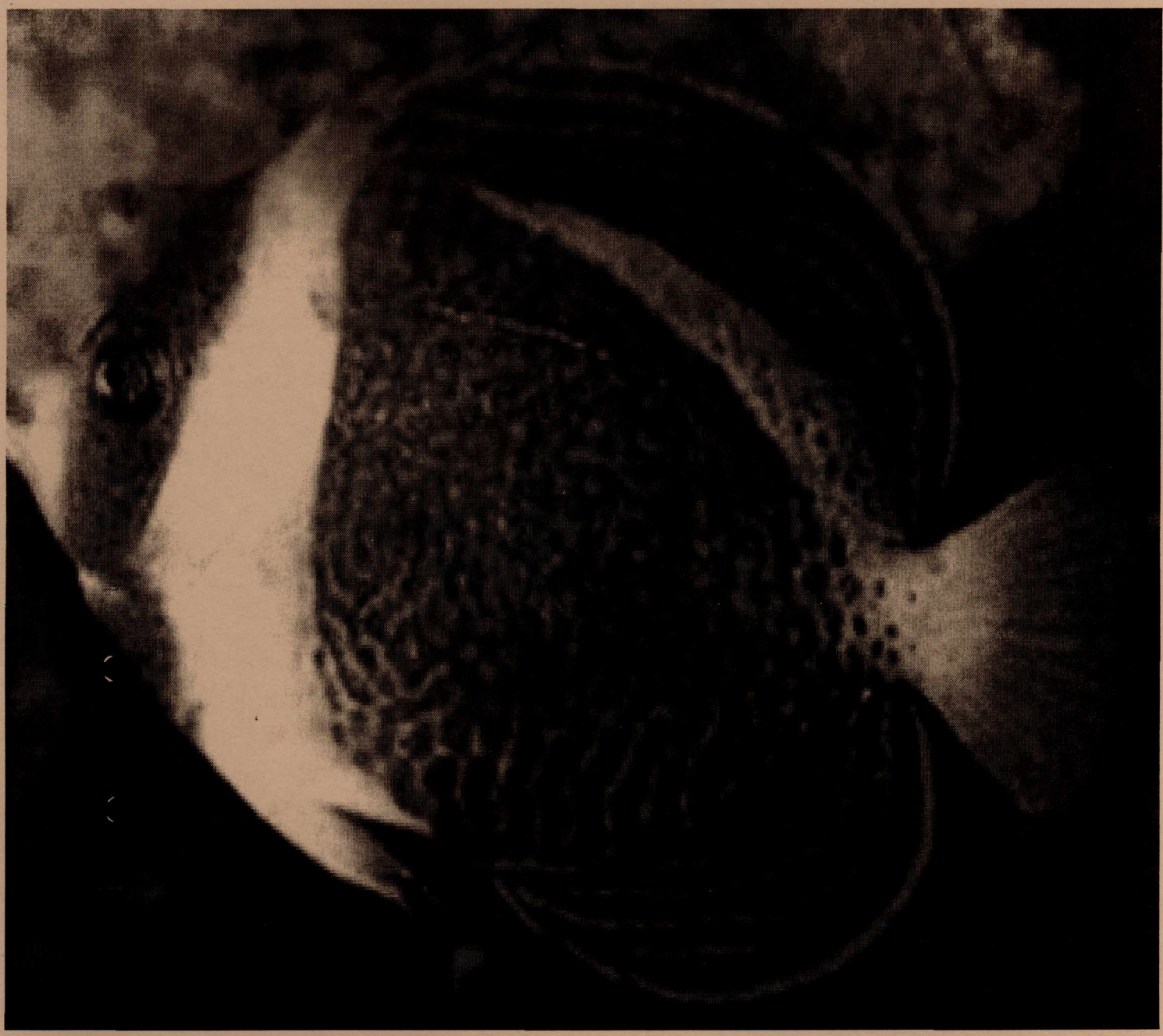

# The Rhodes Journal of Biological Sciences

VOLUME XVIII Spring 2001

**Statement of Purpose:**

The Rhodes Journal of Biological Sciences is a student-edited, annual publication which recognizes the scientific achievements of Rhodes students. Founded seventeen years ago as a scholarly forum for student research and scientific ideas, the journal aims to maintain and stimulate the tradition of independent study. We hope that in reading the journal, other students will be encouraged to pursue scientific investigations and research.

**Editors**

Ellen Barton
Margo Kamel
Kasey Sweeney
Ann Young

**Acknowledgements:** The editors would like to thank Dr. Bobby Jones for his invaluable support and assistance.

---

**RHODES COLLEGE**
**DEPARTMENT OF BIOLOGY**
**2000 NORTH PARKWAY**
**MEMPHIS, TN 38112-1699**
**(901) 843-3561**

*The Rhodes Journal of Biological Sciences*
*VOL. XVIII*

## Table of Contents

# Biology Department Faculty

**Rhodes Biology Faculty:** bottom row, left to right, Dr. Gary Lindquester, Dr. Terry Hill, Christain Hardin, Edith McDowell, Dr. Chuck Stienmetz. Top row, left to right, Dr. Carolyn Jaslow, Dr. David Kesler, Dr. Alan Jaslow, Dr. Thomas Becker, Dr. John Olsen, Dr. Jay Blundon, and Dr. Bobby Jones.

**Dr. Jay Blundon-** For the past 15 years I have been involved in studying biological phenomena associated with communication between neurons. The implications of my research have often been relevant to such diverse areas of neurobiology as neuronal degeneration and regeneration, effects of alcohol on behavior and neuronal function, and mechanisms of learning and memory. My past research has frequently utilized non-mammalian animal models to study synaptic transmission because invertebrate neurons are frequently much larger in size but still show physiological properties similar to mammalian neurons. Research that I am now beginning in my sabbatical year away from Rhodes, in collaboration with molecular biologists in the Department of Developmental Neurobiology at St. Jude Children's Hospital, focuses on the role that cellular proteins play in organizing neuronal synapses into functional units.

Dr. Connie Kurschner at SJCH has recently characterized a neuronal protein (termed NIL-16 for neuronal interleukin-16), found in the mouse cerebellum and hippocampus (both structures involved in learning and memory) that may serve to cluster together several membrane proteins into functional aggregates. Some proteins believed to be grouped together by NIL-16 include potassium and calcium ion channels and glutamate receptors. In addition, NIL-16 contains a protein region which is identical to the immune interleukin IL-16. Further,

neurons that contain NIL-16 also contain IL-16 receptors and the enzyme that has the capability to cleave IL-16 from NIL-16. For at least the next two years, I will be working with Dr. Kurschner to characterize the role of NIL-16 in organizing neuronal membrane proteins, and I will also test whether IL-16 has any influence on synaptic transmission, and perhaps memory formation, in mouse brains.

**Dr. Terry Hill-**After earning a bachelor's degree in Microbiology at the University of South Florida, I began a study of fungal cell development (M.S. and Ph.D., Botany, University of Florida), which I have continued since coming to Rhodes. My early work employed electron microscopical and biochemical approaches to the study of the processes of sporulation and cell growth, and this developed into an interest in the metabolism of fungal cell walls. From a biochemical and cell biological perspective, the cell wall is the most important structural distinction between the cells of animals and fungi, and they are also one of the principal determinants of fungal form and function.

My most recent work in this area has been on the genetics and molecular biology of proteins that reside in fungal walls, as well as cytoplasmic proteins that play roles in determining wall architecture. I and my co-workers have discovered a set of developmental mutants in the fungus *Aspergillus nidulans*, which display evidences of wall abnormalities. Students working on the *Aspergillus* project have performed mating crosses to identify mutants and determine the genetic basis for each mutant phenotype, and future students will continue this approach in order to add more mutant strains to the collection. As well, some students will participate in the planned molecular characterization of the genes responsible for these mutant phenotypes.

**Dr. Alan Jaslow-** I was an undergraduate Zoology Major at the University of Wisconsin in Madison. I earned my MS in Zoology and Ph.D. in Biological Sciences from the University of Michigan. After completing my doctorate I was a postdoctoral fellow at the University of Chicago Department of Anatomy for two years. My research has been focused on the structure and function of vertebrates as well as animal communication. Past research had dealt with the evolution and function of vertebrate middle ears, evolution of male acoustical signals, and the anatomy of mammal leg bones. Students working in my lab have worked with

leg bone shape, flamingo social behavior, prey selection in lizards related to mimicry, spider shape change during development, and sexual differences in tarantula growth energetics.

**Dr. Carolyn Jaslow-** I was an undergraduate Biology Major at Mount Holyoke College. Subsequently, I earned an M.S. in Zoology from Ohio University and my Ph.D. from the Anatomy Department at the University of Chicago. Over the past several years, my research has focused on skeletal biomechanics, specifically, how the morphological designs of mammalian skulls and teeth allow them to accommodate the forces generated during specialized activities of these animals. Recently, I have studied the biomechanics of two features: the cranial sutures and the incisor teeth of rodents. Students working in my lab have carried out experiments investigating how the cranial suture morphology of rats changes during development, and whether those changes are related to bite forces acting on the skull.

**Dr. Bob Jones-** I joined Southwestern at Memphis as an assistant professor of biology in 1968. It was obvious from the onset that I could not continue the research I had started at the University of Missouri because Southwestern did not have the facilities to do genetic research on *Chlamydomas eugametos*. I spent a few summers in the Biochemistry Department at St. Jude Children's Research Hospital before I turned my attention to the genetics of the cotton bowl weevil.

The biology department at the University of Memphis gave me an adjunct appointment around 1975 and I have published papers with three of their faculty. The last paper I published with Dr. Charles Biggers was a chapter in a book and was a summary of 20 years of work. This work was presented at an international meeting in Cardiff, Wales, in 1996.

**Dr. David Kesler-** My research has ranged widely in topics from dealing with freshwater ecology. A long-term research project of mine has been determining the species composition and distribution of freshwater mussels in west Tennessee rivers, especially the Wolf River, where to date we have found 25 species and recorded, using GPS, the locations of over 4,200 individuals. These data are critical for management decisions and formulating regulations to support the river's biota.

Next semester I will work with students looking at glycogen concentration in freshwater mussels of the Wolf River in west Tennessee. Concentration of this storage carbohydrate is an indicator of stress the animals are experiencing. We are testing the prediction that animals in a

reach of the river receiving wastewater effluent will have lower glycogen concentrations than animals living up river from these effluents. Coincident with this research is the investigation of survivorship and growth in the Asian Clam (*Corbicula fluminea)* that we will set out in enclosures. another student research project for next semester will be cataloguing the fishes in a section of Wolf River.

**Dr. John Olsen-** My research interests are connected to the field of Systematics and questions of evolutionary relationships between plants. I have an interest in the ultrastructure of plants, utilizing the scanning electron microscope (SEM) to examine variations in features of plant structures such as pollen grains and "hairs." This has generated a number of student projects since the SEM is a relatively easy instrument to use and generates very interesting images. The most recent project done in this regard has compared SEM and TEM images of cotton fibers.

I am also interested in examining chromosomes, both from the straightforward determination of chromosome number and from the analysis of meiotic chromosome behavior. Our imaging lab provides us with an easy way to capture microscopic images of cells in mitosis and meiosis for evaluation.

Finally, I am interested in secondary plant products, particularly flavoniod compounds. Flavonoid fingerprints are useful systematic tools and we can utilize the HPLC to separate individual compounds from the complex mixture found in the methanolic extracts of leaf or flower tissues.

**Dr. Charles Stinemetz, Department Chair-** Dr. Stinemetz is a former resident of the Buckeye state (Ohio) where he received two BA degrees in Botany & Bacteriology and Chemistry at Ohio Wesleyan University. He was awarded his MS and Ph.D. degrees from The Ohio State University. While in graduate school he became interested in the physiological responses of plants to changes in their environment. His research principally dealt with the role of calmodulin and calcium in root gravitropism and was sponsored by NASA.

Dr. Stinemetz joined the faculty of Rhodes College in 1989 where he has continued to work on response of plants to their environmentincluding both gravitropism and hydrotropism. His work with hydrotropic responses of plants began during a one year sabbatical in Japan which

was sponsored by the Japanese governmental agency MONBUSHO. Each year, Dr. Stinemetz teaches Botany and Mechanism of Developmental Biology. As permitted, he also offers courses in Plant Physiology, Art and Science of Wine, Plants, Genes, and Agriculture, and Space Biology.

Dr. Stinemetz is married and has two children (Nichole-8, and Alex-7). Besides working in the lab and on the computer, he also enjoys movies, Sunday drives, hiking, sports (NBA and college football), wine and gourmet dinning.

## RECENT ADDITION TO THE BIOLOGY DEPARTMENT

**Dr. Mary E. Miller** (will join the Department in the fall of 2001) – My research interests focus on understanding the cell division cycle; primarily the regulatory proteins called cyclins, which are required for cells to faithfully duplicate themselves. Cyclin proteins regulate an essential kinase in the cell, called the cyclin dependent kinase or CDK. Cyclin/CDK complexes are able to phosphorylate proteins and are required for most essential cell cycle events. The cyclin/CDK complexes are controlled at many levels, ranging from transcriptional regulation of the cyclin gene to spatial regulation of the cyclin protein. I am interested in how the spatial regulation of cyclin proteins influence their function and substrate specificity during cell division. This work impacts our understanding of the molecular basis of cell cycle progression; and therefore, the molecular basis of cancer. My research takes advantage of the biochemical, genomic, cytological, and genetic tools available in the budding yeast *Saccharomyces cerevisiae* model system.

I received my B. A. at the University of Tennessee and my Ph.D. at the University of Virginia in microbiology. I have spent the last five years as a post-doctoral fellow at The Rockefeller University where I studied the spatial regulation of cyclin proteins. I will continue this work at Rhodes, where I hope to carry out genetic screens and cytological studies designed to identify cellular proteins that are involved in the spatial regulation of cyclins and potential substrates of the cyclin/CDK complex.

## Science Journal Editors

Ellen Barton, a native of Birmingham, Alabama, is currently a junior at Rhodes College. She is pursuing a double major in Biology and French and hopes to do research abroad after graduation. She also enjoys running, riding horses, traveling and being with her friends.

Margo Kamel is junior biology and political science majors. She is originally from Egypt, and plans to go to medical school. As a Bonner scholar, she volunteers her time at The Med Trauma Center, and she is coordinator of the Hope and Healing Buddies Program. She enjoys reading, traveling, and being with her friends.

Kasey Sweeney is a senior Biology major from Peachtree, Georgia. After graduation, she will be attending medical school.

Ann Young, a native of Shreveport, Louisiana, is currently a sophomore at Rhodes College. She is a biology major, and plans to attend a veterinary school of medicine upon graduation. She is a certified CASA volunteer, and is involved in several campus organizations. Other interests include reading, horseback riding, and camping.

Pictures: group photo, l-to-r, Ann, Margo, & Ellen
*Not pictured:Kasey Sweeney*

## From the Editors

The Editors dedicate this edition of the Journal to our professor and mentor, Dr. Jones.

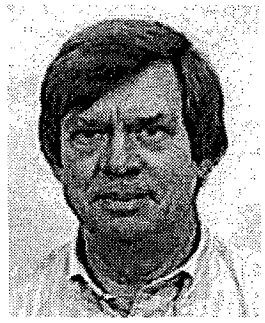

Dr. Bobby Jones (*pictured right*) joined Southwestern at Memphis as an assistant professor of biology in 1968. Over the years, he has served many posts, including that of Chair of the Department. Dr. Robert R. Jones, distinguished Professor of Biology, however, is only one of the many aliases we uncovered. All Rhodes students are aware Dr. Jones is a founding member of the Frazier Jelke Coffee Club, which holds its daily meetings at promptly 3:15 p.m. Some of the readers may be more familiar with Dr. Jones as Framer Jones, the skilled and meticulous custom framer. Others recall the days of his VW Beatle, driven faithfully for so many years. This was only one of the external clues Dr. Jones left of yet another life- that of a record company producer. However, largely, our illustrious professor is most widely known for his tenure as National Chicken Judging Champion. Dr. Jones, whatever guise he may present, has remained a beloved professor among generations of biology students at Rhodes College. A dedicated educator, he will be remembered fondly for his lively and personable lectures and congenial attitude. His classes never lacked a well-timed anecdote or thought-provoking question. For these 33 years of solid and attentive work, the editors dedicate this edition of the journal to Dr. Jones, and wish him many years of happy retirement.

# α-Amylase: Location and Timing in Barley Seed Germination

**Chad Jones**
Rhodes College, 2000 North Parkway; Memphis, TN; 38112

**Abstract:**

In barley seeds, the hormones GA and ABA control the timing of seed germination. This experiment explores the relationship of these two hormones as well as comparing their elicited responses to those of water. Three different techniques are used to quantify the α-amylase response to the 5 various treatments. The first is a bioassay that examines the sensitivities of various hormone/seed segment combinations. The bioassay suggests that the response of aleurone cells to hormonal signaling is greatest in the region surrounding the endosperm. The second section of the experiment is an enzyme activity assay, which compares the starch-consuming potential and protein content of five α-amylase enzyme extracts. Through the α-amylase activity assay, a link is discovered between GA and ABA, implicating a possible mutual role in the stimulation of germination. Finally, a plate gel electrophoresis is used to separate and quantify the proteins in the extracts. Gel electrophoresis supports the other findings as well as establishes the inability of ABA to act alone in aleurone stimulation. These explorations support current ideas about the role of GA, suggest a possible mutual interaction between GA and ABA, and challenge earlier ideas about the sensitivities of varying regions of aleurone tissue to GA.

## Introduction:

In cereal grains like barley, gibberellins (GA) are thought to enhance the synthesis and secretion of the enzyme α-amylase from a layer comprised of aleurone cells surrounding the embryo and endosperm and lining the inside of the seed coat (Ritchie, et al., 1999). In the wild, germination is normally initiated by a specific exposure to light and/or water. The entering of the water into the seed is believed to cause a release of GA from the embryo and the scutellum. The flood of gibberellins permeates through the seed until the hormone reaches the aleurone layer of cells.

α-amylase is not stored in the aleurone layer of the seed; it is made upon request. A signal, thought to be the hormone GA, complexes with a G-protein, and initiates a signal transduction pathway that

binds to the GAI repressor on a GA-MYB gene in the nucleus of the aleurone cell. The mRNA transcript for the gene then exits the cell to direct the protein synthesis of the GA-MYB protein. This protein then initiates the transcription of Amy32b, the α-amylase gene (Lanahan 1992). The mRNA for α-amylase travels to the rough endoplasmic reticulum to initiate protein synthesis of the enzyme α-amylase. The completed enzyme is then secreted by exocytosis. (Plant Physiology 616)

The enzyme α-amylase is a hydrolytic enzyme that breaks down stored molecules within the seed, such as proteins, starch, cell wall structures, and lipids into smaller components. These nutrients can then be transported to the embryo, where they nourish the embryo during germination (Skadsen, 1998).

The inhibition of the α-amylase enzyme is thought to be mediated by another hormone, abscisic acid (ABA) (Skadsen, 1998). Abscisic acid is normally used to regulate seed maturation by increasing the seed's dessication tolerance and preventing the production of α-amylase, thus increasing starch storage longevity (White, et al., 2000). Since GA and ABA act antagonistically throughout other aspects of plant development, it is thought likely that the two hormones act antagonistically in seed germination as well (White, 2000).

In an experiment conducted by White, et al. to test the effects of various levels of GA, they found that an increase in exogenously applied GA concentrations enhanced α-amylase secretion and vacuolation from the aleurone cells.

Additionally, they noticed that the aleurone layer is not equally sensitive in all areas to GA interaction. Their findings revealed that the region of aleurone cells closest to the embryo contains the most cells that are activated under naturally occurring concentrations of GA in germinating grain (White, et al., 1999).

This experiment is designed to test and support these previously-held suppositions concerning the role of GA and ABA in seed germination by an exploration of their effects on barley seeds.

Treatments of the two hormones as well as two time-dependent water treatments and a combination of GA/ABA are applied to various stock of barley seed in three sections of the experiment. Through the use of a bioassay, α-amylase enzyme activity assay, and a gel electrophoresis, multiple aspects of the initiation of seed germination are studied.

This experiment tests the abilities of GA, ABA, and water to elicit the transcription and secretion of α-amylase as well as determine the section of the seed where exogenously applied treatments of the hormones and water cause the greatest release of α-amylase.

## EXPERIMENTAL METHODS

### Bioassay

The bioassay was the first component of the experiment. It allowed the deduction of the hormone that initiates α-amylase activity as well as conduct a determination of the source of α-amylase release in the seed.

The bioassay involves treatment of three types of seed segments with five different therapies, each a possible suspect in the role of inducer of germination. The bioassay reveals which treatment or treatments cause the α-amylase enzyme to be released into the dish media, which contains starch. When α-amylase is released onto the media, it will begin to break down the starch surrounding the seed segment into smaller saccharides.

When the bioassay has completed, the remaining starch is stained, leaving the degraded areas uncolored. These halos of unstained, degraded saccharides can be quantified by area. The data from the quantification can be used to rank the various treatments and seed segments to determine the most likely combination that initiates germination with the release of α-amylase.

To conduct the bioassay, a few hundred barley seeds were soaked in each of the following treatments for the required time, immediately preceding use:

- $10^{-7}$ M GA, 24 hours
- $10^{-7}$ M ABA, 24 hours
- $10^{-7}$ M GA & ABA, 24 hours
- $H_2O$, 24 hours
- $H_2O$, 1 hour.

Then, the barley seeds were dissected bilaterally, and then for some, transversely (Fig. 1) to obtain a collection of three seed sections, "half," "endosperm," and "embryo" for each of the 5 treatments. Five of each section were placed in each of three agar-containing petri dishes, so that a total of 45 plates were laid with seed (9 of each treatment, 3 each of those for each seed section).

The experiment was allowed to run for 7 days, in order to provide time for all released α-amylase to exit the seed section, spread in the dish, and metabolize the starch in the media.

At the end of the experimental period, the seed sections are removed and the starch stained. The remaining unstained areas were counted and measured by area. This bioassay provides a quantitative determination of the effectiveness of the treatment/segment combination.

**Enzyme Activity**

The enzyme activity assay measures the ability of an ∝-amylase enzyme extract to consume a starch substrate. The various rates of substrate conversion are then normalized by dividing by their respective protein contents. The normalization compensates for varying amounts of protein, specifically the α-amylase enzyme, extracted from the seeds.

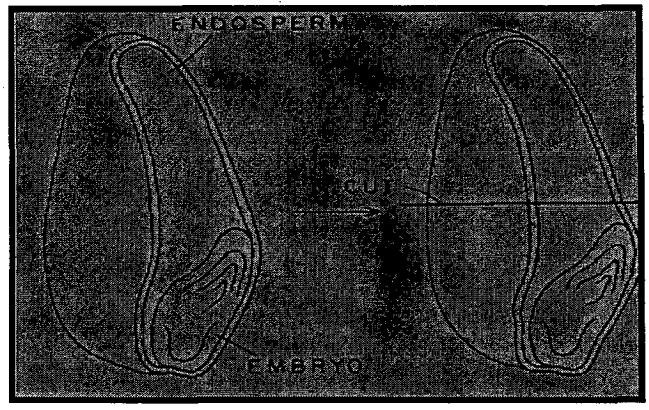


**Fig. 1** – schematic for dissection of seed segments

The enzyme activity assay allows the comparison of amounts of α-amylase released from the seeds by the five seed treatments from the bioassay. Presumably, equal amounts of α-amylase will consume the same amounts of starch. So, the final calculation of enzyme activity will yield values that are the relative amounts of α-amylase released from the seeds for each treatment.

The first step in the enzyme activity assay is the creation of an enzyme extract. This is performed by grinding the seeds in a bath of sodium citrate, so that the α-amylase contained in the seeds will leach into the solvent to form a quantity of enzyme extract. It is important that this extract be kept cold during the duration of the entire experiment, for the enzyme is temperature-sensitive.

The enzyme extract is then used as a source for the two parts of the experiment: enzyme activity and protein content.

The enzyme activity experiment is performed by making multiple dilutions of the extract (1/10, 1/50, 1/100, etc.), as well as positive and negative controls. The positive control is made with the standard amount of starch and HCl added at the beginning of reaction to deactivate the α-amylase. The negative control is made of active α-amylase, but contains a buffer solution instead of the starch solution. At the end of 10 minutes, the reaction is halted by the addition of HCl to all dilutions, and iodine is added to stain the remaining, unconsumed starch. Samples of each dilution are loaded into a cuvette and inserted into a spectrophotometer. The absorbance at 580 nm is read as a percent of the scale between the negative control (0 %), and the positive control (100%).

The protein content is determined with the use of the Biuret Reaction, in which the copper ions in the biuret reagent complex with peptide bonds in the proteins to produce a purple color. The actual determination of protein content is made by comparing absorbencies of various dilutions of biuret-protein complex with a standard curve. The standard curve (Fig. 6) is generated by plotting the absorbance of known concentrations of a biuret-protein complex. The line running through these plotted points is the standard curve.

To determine the protein concentration of the unknown protein extract, various dilutions are made until one registers an absorbance along the standard curve. The x-axis value of the intersection point is the amount of protein, in mg/mL, of the diluted solution.

**Gel Electrophoresis**

The final section of the experiment is another quantification of protein content using gel electrophoresis. In the gel electrophoresis, unwound, polarized proteins are forced through the thick gel plate media by an electric field. This procedure allows the proteins contained in the sample to be separated by size, for the smaller proteins will move farther down through the gel than the larger proteins that have a more difficult time moving through the thick polymerized substance.

A quantification of protein contained in the sample is obtained by finding the area of the gel that the proteins occupy. By comparing the areas of protein among the five treatments, another determination can be made as to which treatment induced the greatest amount of α-amylase production in the seeds.

The gel electrophoresis is carried out with standard SDS gel preparation. Then, a 10 µL sample of each extract, each representing one of the initial treatments, is loaded into the flooded gel plate. An electric field is allowed to pass over the plates, forcing the proteins down through the gel. Upon completion, the amount of protein is ascertained by use of measuring and area calculation.

## RESULTS

### Bioassay

The bioassay was quantified by counting the number of halos present in each dish, and calculating the average area for one halo in each treatment/seed segment. Additionally, the total halo area per treatment/segment is calculated to compare the total activity in the bioassay. Graphical results are shown in Fig. 2 – Fig. 4.

The determination of halo size is made by measuring the diameter of the halo, beginning and ending at the boundary of the stained starch. (Fig 5)

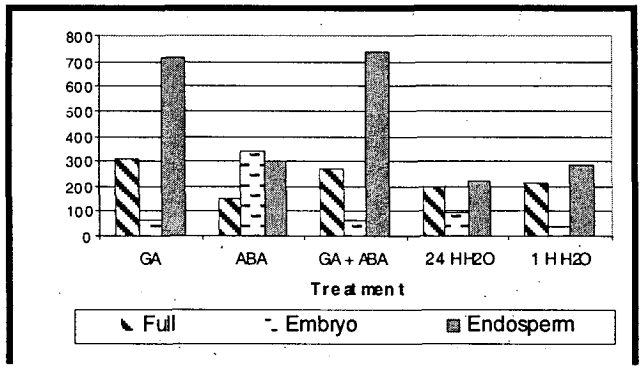


**Fig. 3** – The average halo area for each treatment/segment

The number of halos is fairly consistent between the full and endosperm seed sections. In all but the ABA treatment, the embryo region produced far fewer halos.

The average halo size, which reflects the amount of α-amylase released into the dish, was greater for the endosperm than the full. The full sections produced larger average halos in GA, GA & ABA, 24h $H_2O$, and 1h $H_2O$, but smaller halos than the ABA.

The results of the total area calculation of the bioassay show that in 4 of the 5 treatments, the endosperm region released more α-amylase than either the embryo quarter or complete seed half.

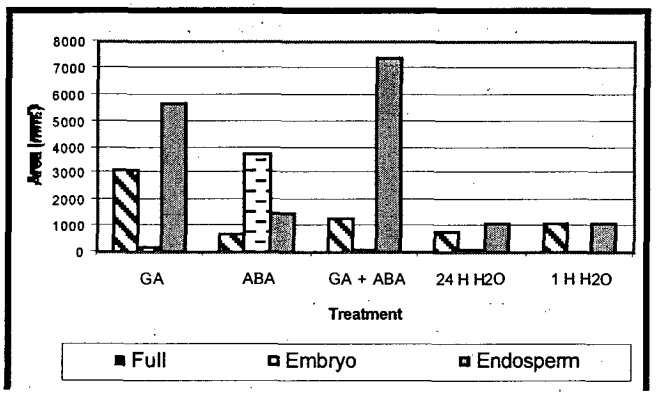


**Fig. 4** – The total halo area for each treatment/segment.

**Fig. 5** – Dish containing stained starch and two clearly evident halos

## Enzyme Activity

The enzyme activity assay is comprised of two separate calculations: the protein content and enzyme activity.

The standard curve for the determination of protein content (Fig. 6) is generated with known amounts of BSA (bovine serum albumin). Various amounts of protein in solution are measured for absorbance in a spectrophotometer and recorded for the independent value of the curve. The amount of protein, in mg/mL, is the dependent variable. By obtaining a concentration of unknown amounts of protein that register an absorbance along the curve, the corresponding x-axis value of protein content in that dilution can be determined. This is done by multiplying the dilution factor by the amount of protein in the dilution. For example, a 1/10 dilution of extract that returns a protein content of .5 would indicate a total protein content of the extract as 5 mg/mL.

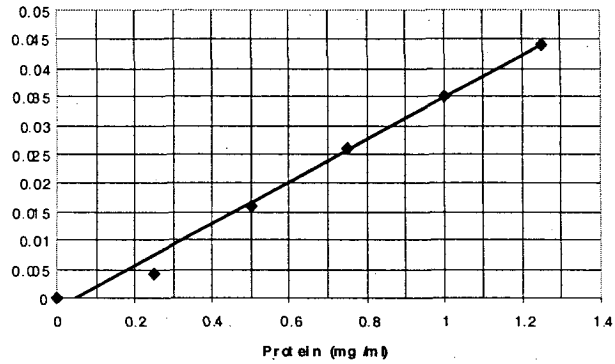


**Fig. 6** – Standard curve for protein content determination.

The determination of _-amylase activity is conducted by the use of a continuous absorbance scale bounded at the bottom by the absorbance of the negative control and the top by the positive control.

Increasing amounts of enzymatic activity will cause a greater amount of starch degradation. The percent relative absorption of a concentration of α-amylase enzyme extract coincides with the same percentage of starch remaining in the assay, of the original 2 mg starch in solution.

Dilutions that consumed ~90% of the starch or more were considered to be saturated, and were not used for later calculations. Instead, a more dilute concentration is used, until the amount of starch consumed nears 50%.

With the known enzyme activity and protein amounts, the final calculation reveals the effectiveness of the initial treatment in inducing the release of α-amylase from the seed. The total enzyme activity for each treatment is calculated by using the formula:

$$\text{Total Enzyme Activity} = \frac{\left(\frac{\%\ \text{starch consumed} \leftarrow 2\text{mg starch}}{\text{dilution}}\right)}{\text{protein content}}$$

Values obtained for % starch consumed, dilution factor, protein amount, and total enzyme activity are displayed in Fig. 7.

The results in this section show that the combination of GA and ABA have a much higher total enzyme activity than any of the other 4 treatments, followed by 24h $H_2O$ and then GA.

## Gel Electrophoresis

The gel electrophoresis (Fig. 8) allows a further determination and quantification of the protein in the extract solutions.

| Treatment | % Starch | Dilution | Protein (mg/mL) | Tot. Act. |
|---|---|---|---|---|
| 24 h H2O | 44.1 | 1/100 | 25 | 3.53 |
| 1h H2O | 62 | 1/50 | 112 | .55 |
| GA | 73.7 | 1/100 | 110 | 1.34 |
| ABA | 51 | 1/10 | 21 | .49 |
| GA & ABA | 79 | 1/1000 | 20 | 79 |

**Fig. 7** – The data obtained and resultant total activity calculations for the five treatments in the enzyme activity assay

The quantification of the results of the gel electrophoresis (Fig. 9) is performed by comparing the areas of the protein smears through the gel. The calculations show that the ABA/GA and GA treatments produce greater protein areas on the gel plate than the ABA, 24h $H_2O$, and 1h $H_2O$.

**Conclusions:**

The most surprising result from the bioassay suggests a different location of maximum α-amylase stimulation from the area observed by White, et al.. The bioassay clearly shows that the number of halos, representing the number of seed segments that positively responded to the treatment, are much greater for four of the treatments in the entire half seed and the region of the endosperm than the embryo.

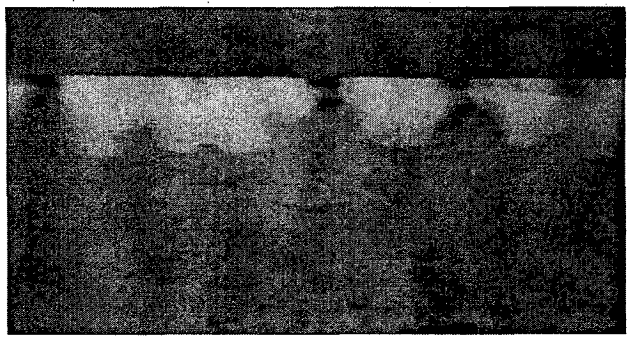

**Fig. 8** – The final gel plate after the electrophoresis had been allowed to run for ~6 hours. The vertical dark stripes extending down from the horizontal dark/light boundary line are the continuum of stained proteins. Left to right, the stripes are: ABA/GA, ABA, GA, 1h $H_2O$, and 24h $H_2O$.

| Treatment | Approx. Area Units |
|---|---|
| ABA/GA | 120 |
| ABA | 0 |
| GA | 105 |
| 1h $H_2O$ | 30 |
| 24h $H_2O$ | 50 |

**Fig. 9** – Table of the approximate area of protein coverage from gel electrophoresis

The quantification of the average halo size for each treatment/segment yielded greater values for the endosperm than the entire seed half for the two treatments that contain GA. This means that the sections that responded positively to the treatments initiated a greater release of α-amylase from the aleurone cells.

The total halo area calculation incorporates the first two quantifications to create a more valid comparison of the total stimulated ∝-amylase release. Clearly, the experimental data shows that the most active combination of treatment/seed segment are those containing GA in the region of the endosperm.

An area of concern in the bioassay is that of the embryonic regions of the ABA treatment. The information concerning what is known about the role of ABA does not support such a finding. Also, the results are not consistent with the other ABA data and the GA/ABA data. Because of these incongruities, it is likely that some error in seed dissection or management caused the inconsistent values.

The data from the enzyme activity assay does support the theory that GA stimulates _-amylase release more than does ABA. The 1.34 to .49 total activity, respectively, is nearly a 3:1 ratio which holds in favor of GA.

As one would expect, the 1h $H_2O$ did not cause much activity, though it was ahead of ABA. The 24h H2O, on the other hand, produced more than twice the activity of GA. This might suggest that the seed's own release of GA in response to a perceived environmental stimulation for germination is greater than the absorbed GA from the exogenous application. It is also possible that these findings illuminate a problem with the GA treatment, whether in application or measurement.

Of a highly interesting note, the activity of GA/ABA was nearly one hundred fold the activity of the others. Such a great value might show that GA and ABA somehow work together to initiate seed germination by eliciting an eruption of α-amylase when the two hormones are in agreeable concentrations.

Still, the α-amylase activity assay supports previous notions that GA initiates seed germination while ABA works to inhibit the pro-action. Also, this section of the experiment highlights the importance of water and the specialization of the natural processes which usually function outside of the laboratory to signal seed germination.

The gel electrophoresis is helpful to assess enzyme content by creating a visual blot of the contained proteins in the 5 extracts. The data from the area quantification of the gel blots shows ABA to have no effect on α-amylase while confirming the results from the enzyme activity assay implicating GA/ABA as the dominant elicitor of α-amylase secretion. The levels of proteins caused by GA are nearly as great as those of GA/ABA, and much greater than the 1h $H_2O$, 24h $H_2O$, and the ABA.

The merging of data from the three sections of the experiment confirms some of the previous studies on seed germination and refutes others. Throughout the trials, GA has shown dominance over ABA in the initiation of seed germination by causing the release of α-amylase from the aleurone cell layer.

Interestingly, this experiment suggests that ABA might have a role with GA in this process, and that further studies need to be conducted to determine the ways in which ABA and GA interact within the seed. Water was also shown to be a method of propagating seed germination, though not as actively as external hormone solutions containing GA.

Finally, of prime significance is the experimental support for the possibility that α-amylase release is greatest in the region of aleurone tissue surrounding the endosperm alone. While this result is contrary to earlier studies, it is a valid possibility because of the massive amounts of starch in the endosperm.

Were α-amylase levels to be greatest surrounding the embryo, there would be no immediate source of substrate for the enzyme to degrade. Therefore, it is both intuitive and experimentally shown that GA acts with the endosperm-surrounding aleurone cells to cause the greatest synthesis and secretion of α-amylase.

## References

Lanahan MB, Ho TH, Rogers SW, Rogers JC (1992) A gibberellin response complex in cereal alpha-amylase gene promoters. The Plant Cell **4:** 203-211

Ritchie S, McCubbin A, Ambrose G, K T, Gilroy S (1999) The Sensitivity of Barley Aleurone Tissue to Gibberellin is Heterogeneous and May Be Spatially Determined. Plant Physiol 120: 361-370

Skadsen R (1998) Physiological and molecular genetic mechanisms regulating hydrolytic enzyme gene expression in cereal grains. US Dept Agr. http://www.nalusda.gov/ttic/tektran/data/000009/40/0000094037.html

Taiz L. and E. Zeiger, *Plant Physiology* (2nd ed.), Chap. 20. Sunderland, MA: Sinauer Associates, Inc., 1998.

White C, Proebsting W, Hedden P, Rivin C (2000) Gibberellins and Seed Development in Maize. I. Evidence That Gibberellin / Abscisic Acid Balance Govern Germination versus Maturation Pathways. Plant Phys **122**: 1081-1088

# Changes in Rat Cranial Suture Morphology

Dr. Carolyn Jaslow and Brock Lanier
Rhodes College, Department of Biology
2000 N. Parkway; Memphis, TN 38112

**Abstract:**

Cranial sutures are joints between the skull bones and their structure reflects patterns of growth and applied forces. To examine the effect of incisor eruption and occlusion on the developing suture, thirty-six rat pups were sacrificed on days one, five, seven, nine, thirteen, seventeen, and twenty-three of life. The skulls of these rats were cleared and stained. Facial sutures of the skulls were measured and the complexity, or interdigitation, of these sutures was quantitatively recorded as the ratio of the length of the suture divided by its end-to-end distance. These measurements can illustrate whether a linear development of interdigitation occurs or if the rate of interdigitation is related to incisor eruption, which begins between days eight and ten, and the start of occlusion, which begins a few days later.

**Introduction:**

The development of the vertebrate skull is an incredibly intricate and complex process that has been the subject of extensive embryological study. Cranial bones take shape and begin growing during gestation and do not reach maturity until some time after birth (Markens 1975; Moss, 1954; Pritchard *et al.*, 1956). A widely accepted model proposed by Pritchard *et al.* ascribes five steps to the developmental process (Pritchard *et al.*, 1956). The first such step occurs as the opposing bones first form, grow, and approach one another. The meeting of the bones is the second stage. These resulting junctures are known as sutures and are composed of connective tissues that join adjacent bone. Five tissue layers separate the opposing cranial bones and two hold together the bones at the plane of articulation, or the location at which the suture is perpendicular to the bones' surface. Throughout the following developmental phases – the early, late, and adult periods - these tissue layers increase or decrease in thickness, mitotic activity eventually slows, and vascularization occurs amidst the large array of physiological and morphological changes that ultimately produce a pair of stable bone edges forming a distinct suture. Both the rate and the amount of time until closure differ, even within species, but the same sequence always occurs (Pritchard *et al.*, 1956; Wagemans *et al.*, 1988).

The role of the suture, whether it is either the generally undifferentiated soft tissue surrounding the developing cranial bones or the "relatively well differentiated tissue" (Moss, 1954) found at the plane of articulation of adult bones, has been the subject of extensive scientific study and debate. It has been proposed that "the sutures in the skull have several functions. They unite bones, they absorb forces, they act as joints that permit relative movement between bones, and they play a role as growth sites in the growing skull," (Wagemans *et al.*, 1988). Two predominant, opposing views have been offered to explain which factors most heavily influence this process of cranial bone growth and developmental suture morphology. One states that the sutures grow and are shaped autonomously by predetermined, genetic factors. The other maintains that introduced, environmental forces have the greatest influence (Moss, 1957; Moss, 1975; Oudhof 1982; Roth *et al.*, 1996; Wagemans *et al.*, 1988). Several studies, for example, have supported the notion that intracranial pressures precipitate sutural growth more than pre-determined genetic factors (Levine *et al.*, 1998; Oudhof and van Doorenmaalen, 1983; Pritchard *et al.*, 1956).

Other investigations focus on the organismal morphology and functionality of the suture. A common belief correlates increasing sutural complexity, or greater interdigitation, with the presence of stronger forces exerted on the cranium. Such forces may either be intrinsic, such as intracranial pressure, or extrinsic, such as head butting. It has also been noted that sutures seem to simply become increasingly interdigitated with time (Wagemans *et al.*, 1988). However, no study has ever quantitatively recorded the complexity of a developing cranial suture.

This investigation quantitatively examines the dynamic sutural changes in complexity of the rat cranium as it develops from birth until weaning, which occurs on approximately day twenty-one of the rat's life. This study focuses on the relationship that the complexity exhibited by the premaxillary/frontal suture shares with the emerging forces introduced by the eruption and occlusion of the incisor. The premaxillary/frontal suture is found at the junction between the cranial frontal bone and the facial premaxillary bone, which connects directly to the animal's large incisor (figure 1 and 2). The development of neighboring nasal/frontal suture is used as a control because it is situated directly next to the premaxillary bone, but is not joined to the emerging teeth. It, therefore, is not introduced to the forces associated with tooth eruption and occlusion. The sutural complexity, or interdigitation, exhibited by the rat's skull is quantitatively recorded as the ratio of the length (L) of the suture divided by its end-to-end distance (D), (i.e.

L/D value) (figure 3). This study proposes that the emerging forces generated from the introduction of the chewing and biting of the occluding incisor will increase the rate of interdigitation of the premaxillary/frontal suture.

**Methods:**

Eruption of the incisor is expected on approximately day seven and occlusion a few days thereafter. If the hypothesis is correct, the rate of the interdigitation of the premaxillary/frontal suture ought to dramatically increase during incisor occlusion, which was estimated to follow a few days after eruptions (i.e. between the tenth and twelfth days of life). Figure 4 illustrates this theoretical development graphically. According to this model, the nasal/frontal suture's complexity ought to develop independent of the introduced forces of the incisors, which are not applied to the nasal/frontal suture. Quantifying and comparing the morphological changes that these sutures experience during the organism's development shows whether or not a correlation exists between the sutural morphology and the introduction of an extrinsic force. This will help to determine whether or not sutural growth and morphology are the result of a genetically programming sequence or the product of environmental factors. Such information can be extremely useful in evaluating cranial morphology, especially fossil morphology for which there exists no functional record of the skull.

The desired data was obtained by sacrificing thirty-four rat pups with injections of sodium pentobarbital on the first, third, fifth, seventh, ninth, thirteenth, seventeenth, and twenty-third days of life. The days selected for sacrificing the animals represent fairly regular intervals throughout the rat's period of weaning, which is completed on approximately the twenty-first day of life. Particular attention was given to collecting more data points on days seven, nine, and thirteen due to the anticipated increase of complexity during this period.

The skulls of the specimens were cleared and stained so that both sutures from each specimen could be easily discerned. Using a dissecting scope fitted with a drawing tube, the sutures were reproduced two-dimensionally onto paper. Five traces of each suture from each skull were made. Each of these five traces was then digitized using the MacMeasure program. The computer in turn quantitatively measured and calculated the sutures' lengths and distances, producing the desired complexity coefficient. The five (L/D) values of each suture were then

averaged to produce the (L/D) values for each set of data, the premaxillary/frontal and the nasal/frontal sutures (appendix, tables 1 and 2).

**Results:**

After plotting the data from each type of suture, trendlines that best described the data were obtained by comparing the regressions of linear, second order polynomials, third order polynomials, etc. The optimal trendline utilizes the lowest order of coefficients necessary to offer the best fit, as calculated by the $R^2$ value. Accordingly, it was determined that the third and second order polynomials best described the data of the premaxillary/frontal suture and the nasal/frontal suture, respectively (figures 5 and 6).

The effects of gender on the rate of interdigitation of each suture was compared by plotting the interdigitation values (i.e. L/D ratios) of each gender (figure 7 and 8). Neither suture exhibited any appreciable differences in this respect.

**Discussion:**

The interdigitation values of the two sutures were then plotted together and compared (figure 9). The results refute the experiment's original hypothesis, which states that the introduction of forces will increase the rate of interdigitation. Events that were predicted to have an impact on the rate the suture's development did not exhibit the anticipated influence. As is apparent from figure 9, the rate of interdigitation of the premaxillary/frontal suture proceeds in a rather linear fashion once it begins to increase on approximately day seven of the rat's life. No change in the rate of interdigitation of the premaxillary/frontal suture is observed on day thirteen, the anticipated time of incisor's occlusion. It is noted that in some of the specimens occlusion took place later than expected, at a point in between thirteen and seventeen days old. However, this developmental period maintains the linear interdigitation trend. The nasal/frontal suture develops in a likewise manner, maintaining a steady rate of increasing complexity once the suture begins to interdigitate. However, the nasal/frontal suture is noted to be slower than its counterpart in initiating this process. The data ultimately indicates that the development of the cranial bones and their sutures is more likely due to genetic factors rather than environmental ones.

## References

Farris EJ and Griffith JQ. The Rat in Laboratory Investigation. New York: Hafner Publishing, 1967.

Levine JP, Bradley JP, Roth DA, McCarthy JG, and Longaker MT. Studies in cranial suture biology: regional dura mater determines overlying suture biology. Plast. Reconstr. Surg. 101: 1441-11447 (1998).

Markens MS. Embryonic development of the coronal suture in man and rat. Acta. Anat. 93 (2): 257-273 (1975).

Moss ML. Growth of the calvaria in the rat. Am. J. Anat. 94: 333-361 (1954).

Moss ML. Experimental alteration of sutural area morphology. Anat. Rec. 127: 569-590 (1957).

Moss ML. Functional anatomy of cranial synostosis. Childs Brain 1: 22-33 (1975).

Oudhof HAJ. Sutural growth. Acta. Anat. 112: 58-68 (1982).

Oudhof HAJ and van Doorenmaalen WJ. Skull morphogenesis and growth: hemodynamic influence. Acta. Anat. 117: 181-186 (1983).

Pritchard JJ, Scott JH, and Girgis FG. The structure and development of cranial and facial sutures. J. Anat. 90: 73-86 (1956).

Roth DA, Bradley JP, Levine JP, McMullen HF, McCarthy JG, and Longaker MT. Studies in cranial suture biology: part II. Role of the dura in cranial suture fusion. Plast. Reconstr. Surg. 97: 693-699 (1996).

Wagemans PAHM, van de Velde JP, and Kuijpers-Jagtman AM. Sutures and force: a review. Am. J. Orthod. Dentofac. Orthop. 94: 129-141 (1988).

## Appendix

**Table 1: Premaxillary/Frontal data**

| age (days): | rat ID: | (L/D) |
|---|---|---|
| 1 | 1dayF4A | 1.062 |
| 1 | 1dayF4B | 1.088 |
| 1 | 1dayF2 | 1.108 |
| 1 | 1dayF3 | 1.074 |
| 5 | 5dayF4 | 1.31 |
| 5 | 5dayF2 | 1.108 |
| 5 | 5dayF3A | 1.16 |
| 5 | 5dayF3B | 1.084 |
| 7 | 7dayF4 | 1.218 |
| 7 | 7dayF2 | 1.44 |
| 7 | 7dayF3A | 1.198 |
| 7 | 7dayF3B | 1.222 |
| 7 | 7dayF3C | 1.362 |
| 9 | 9dayF4A | 1.368 |
| 9 | 9dayF4B | 1.62 |
| 9 | 9dayF2A | 2.376 |
| 9 | 9dayF2B | 2.3 |
| 9 | 9dayF3 | 1.9 |
| 13 | 13dayF4A | 3.658 |
| 13 | 13dayF4B | 4.526 |
| 13 | 13dayF4C | 4.306 |
| 13 | 13dayF2A | 4.098 |
| 13 | 13dayF2B | 4.412 |
| 13 | 13dayF2C | 5.06 |
| 17 | 17dayF4A | 4.466 |
| 17 | 17dayF4B | 5.576 |
| 17 | 17dayF2A | 7.224 |
| 17 | 17dayF2B | 6.052 |
| 17 | 17dayF2C | 5.686 |
| 23 | 23dayF4A | 8.014 |
| 23 | 23dayF4B | 8.734 |
| 23 | 23dayF2A | 10.902 |
| 23 | 23dayF2B | 10.086 |
| 23 | 23dayF2C | 6.796 |

**Table 2: Nasal/Frontal data**

| age (days): | rat ID: | (L/D) |
|---|---|---|
| 1 | 1dayF4A | 1.238 |
| 1 | 1dayF4B | 1.238 |
| 1 | 1dayF2 | 1.132 |
| 1 | 1dayF3 | 1.076 |
| 5 | 5dayF4 | 1.13 |
| 5 | 5dayF2 | 1.166 |
| 5 | 5dayF3A | 1.098 |
| 5 | 5dayF3B | 1.118 |
| 7 | 7dayF4 | 1.196 |
| 7 | 7dayF2 | 1.116 |
| 7 | 7dayF3A | 1.41 |
| 7 | 7dayF3B | 1.132 |
| 7 | 7dayF3C | 1.126 |
| 9 | 9dayF4A | 1.196 |
| 9 | 9dayF4B | 1.148 |
| 9 | 9dayF2A | 1.126 |
| 9 | 9dayF2B | 1.11 |
| 9 | 9dayF3 | 1.122 |
| 13 | 13dayF4A | 1.556 |
| 13 | 13dayF4B | 2.838 |
| 13 | 13dayF4C | 2.35 |
| 13 | 13dayF2A | 2.794 |
| 13 | 13dayF2B | 2.746 |
| 13 | 13dayF2C | 2.38 |
| 17 | 17dayF4A | 2.062 |
| 17 | 17dayF4B | 2.568 |
| 17 | 17dayF2A | 3.69 |
| 17 | 17dayF2B | 2.104 |
| 17 | 17dayF2C | 1.82 |
| 23 | 23dayF4A | 2.596 |
| 23 | 23dayF4B | 4.186 |
| 23 | 23dayF2A | 7.374 |
| 23 | 23dayF2B | 7.952 |
| 23 | 23dayF2C | 3.338 |

**Figure 1: Dorsal view of rat cranium**

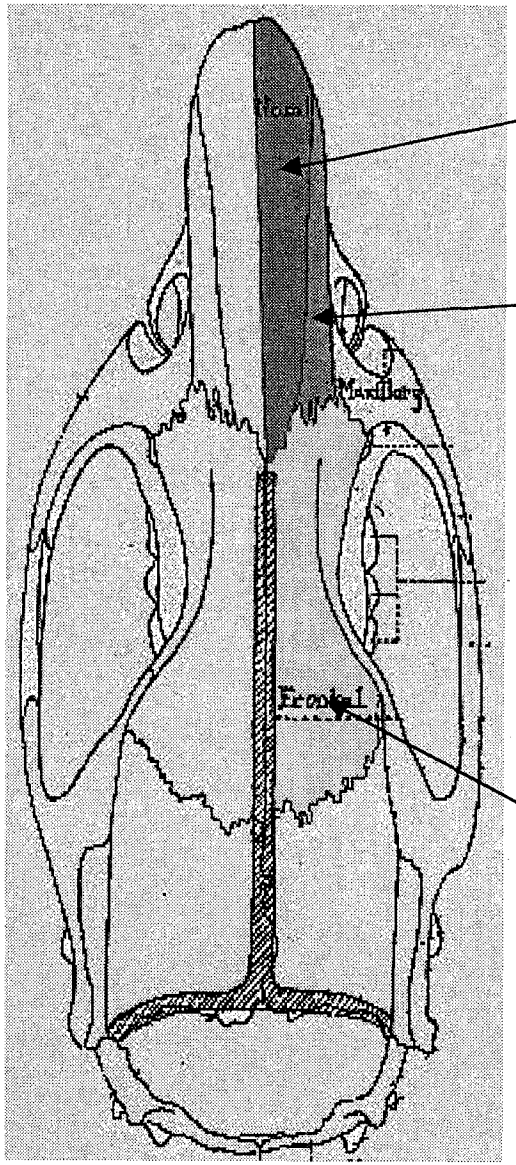


**Figure 2: Lateral view of rat cranium**

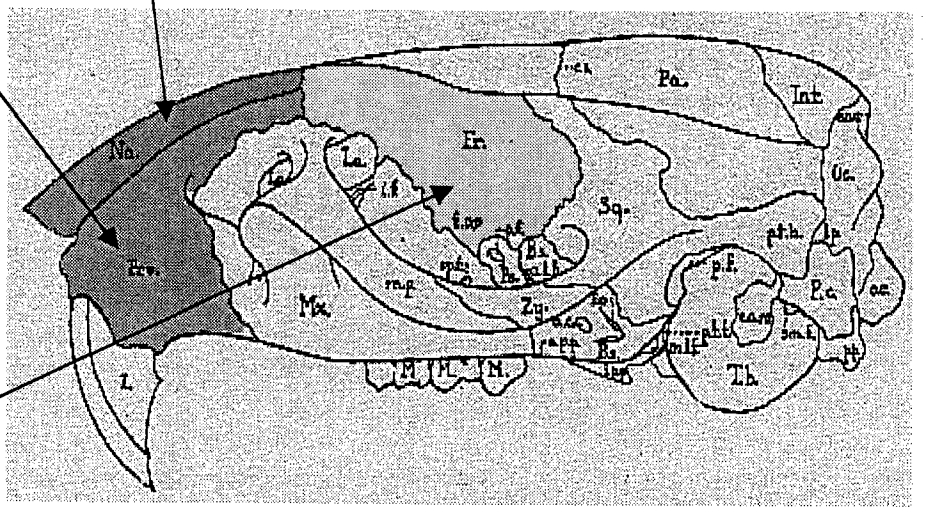

**From Farris and Griffith, 1967**

**Figure 3: Illustration of hypothetical suture's length to distance (L/D)**

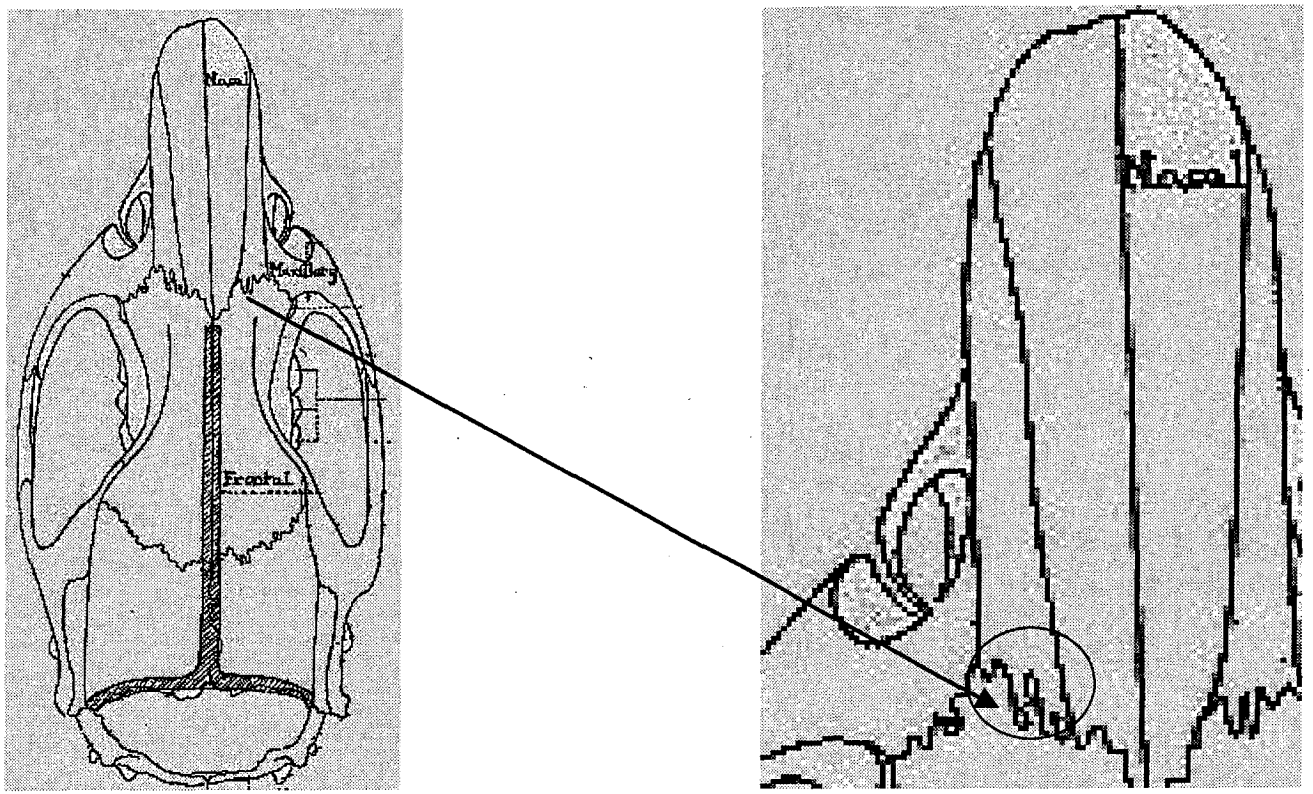


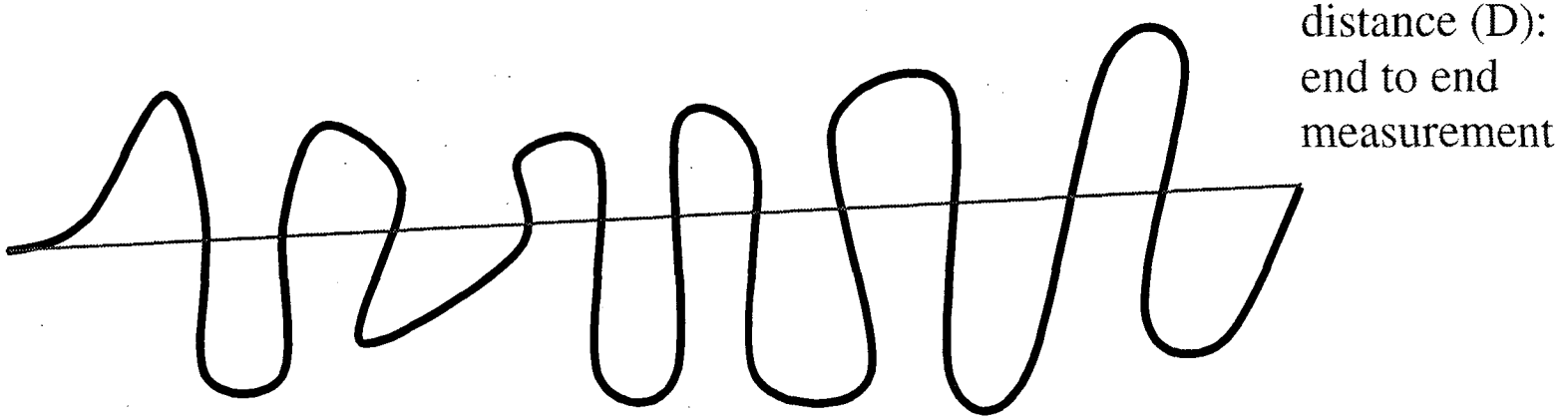

distance (D):
end to end
measurement

# Figure 4: Theoretical interdigitation v. time

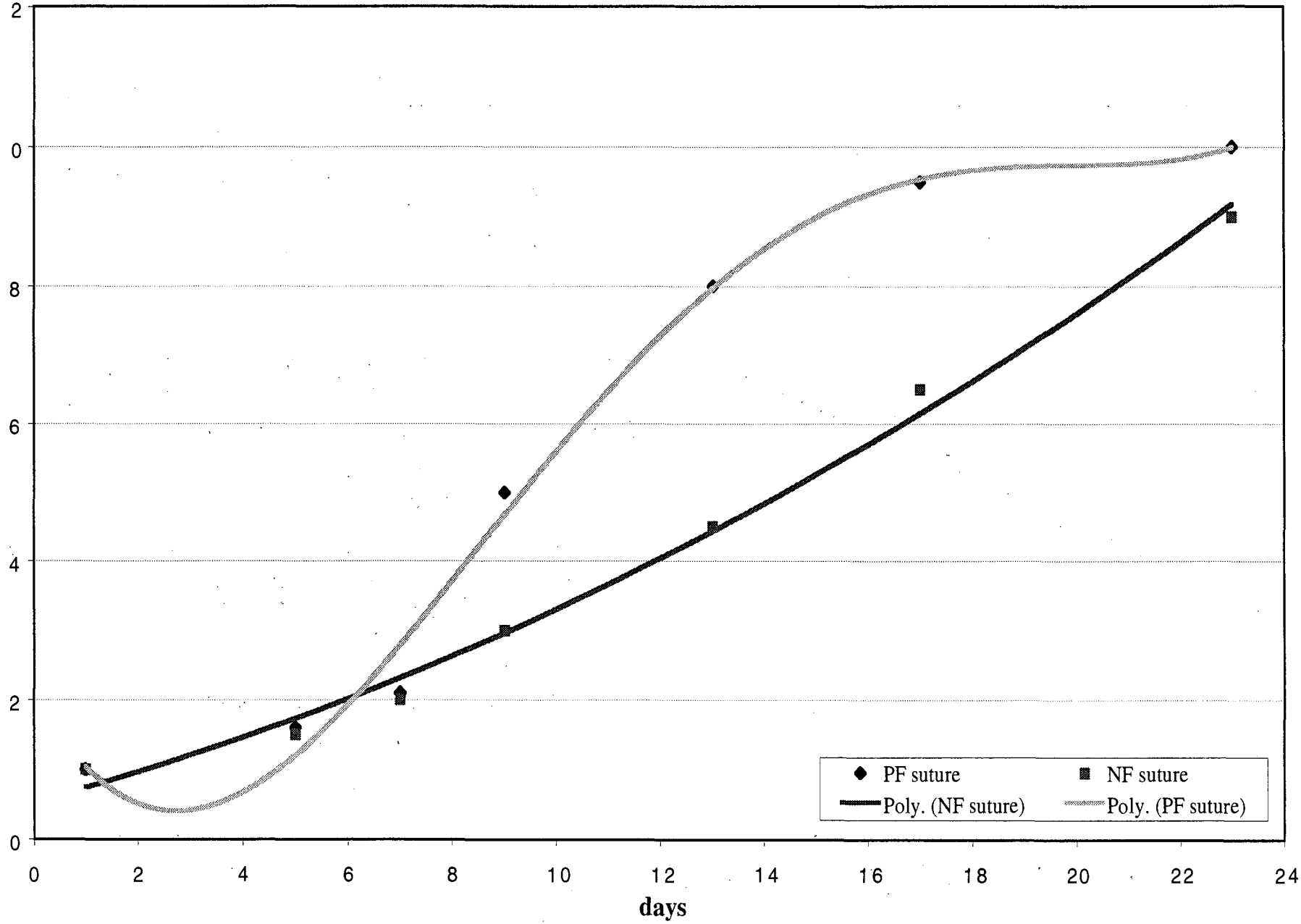

# Figure 5: Premaxillary/Frontal suture trendline comparison

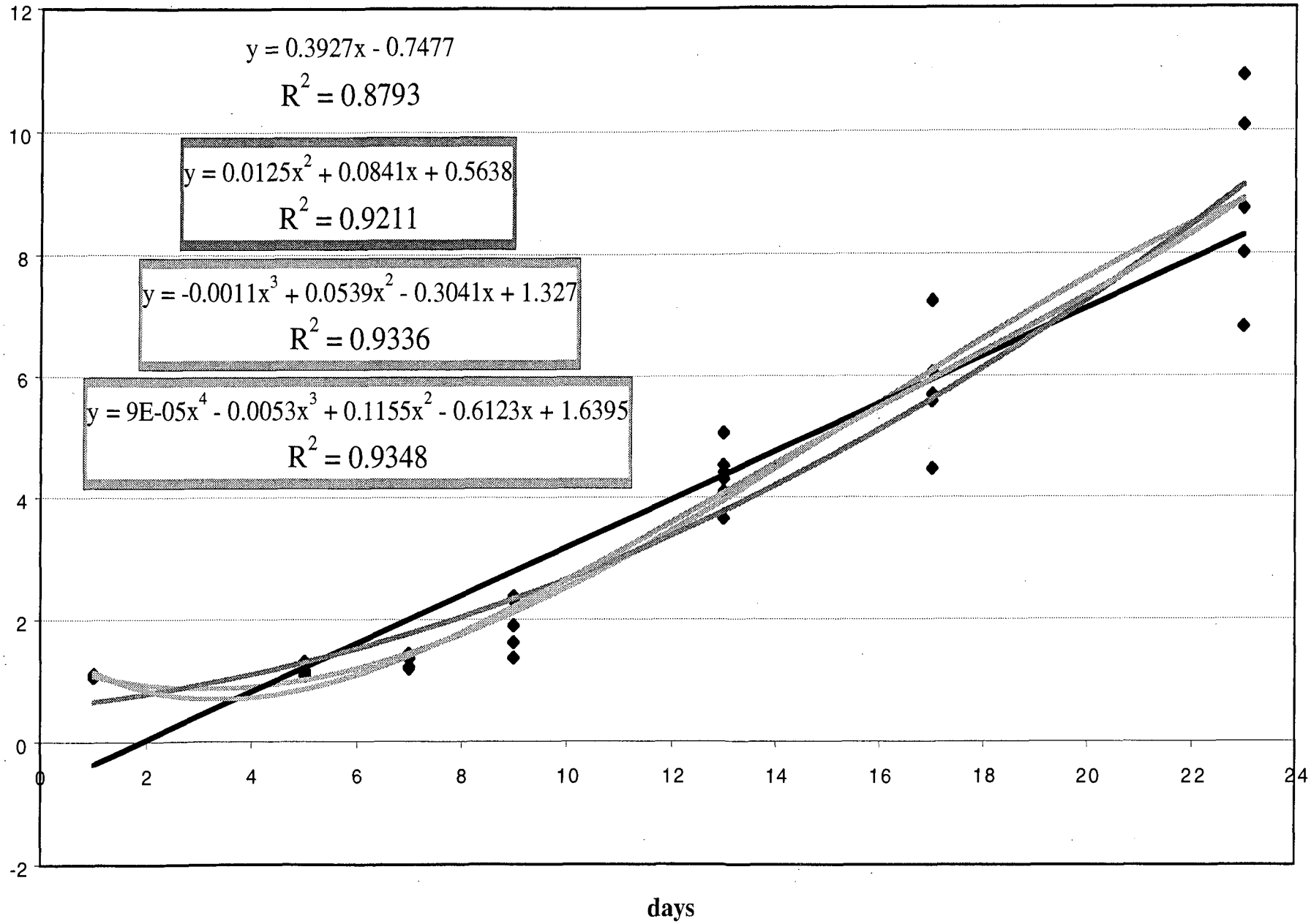

# Figure 6: Nasal/Frontal suture trendline comparison

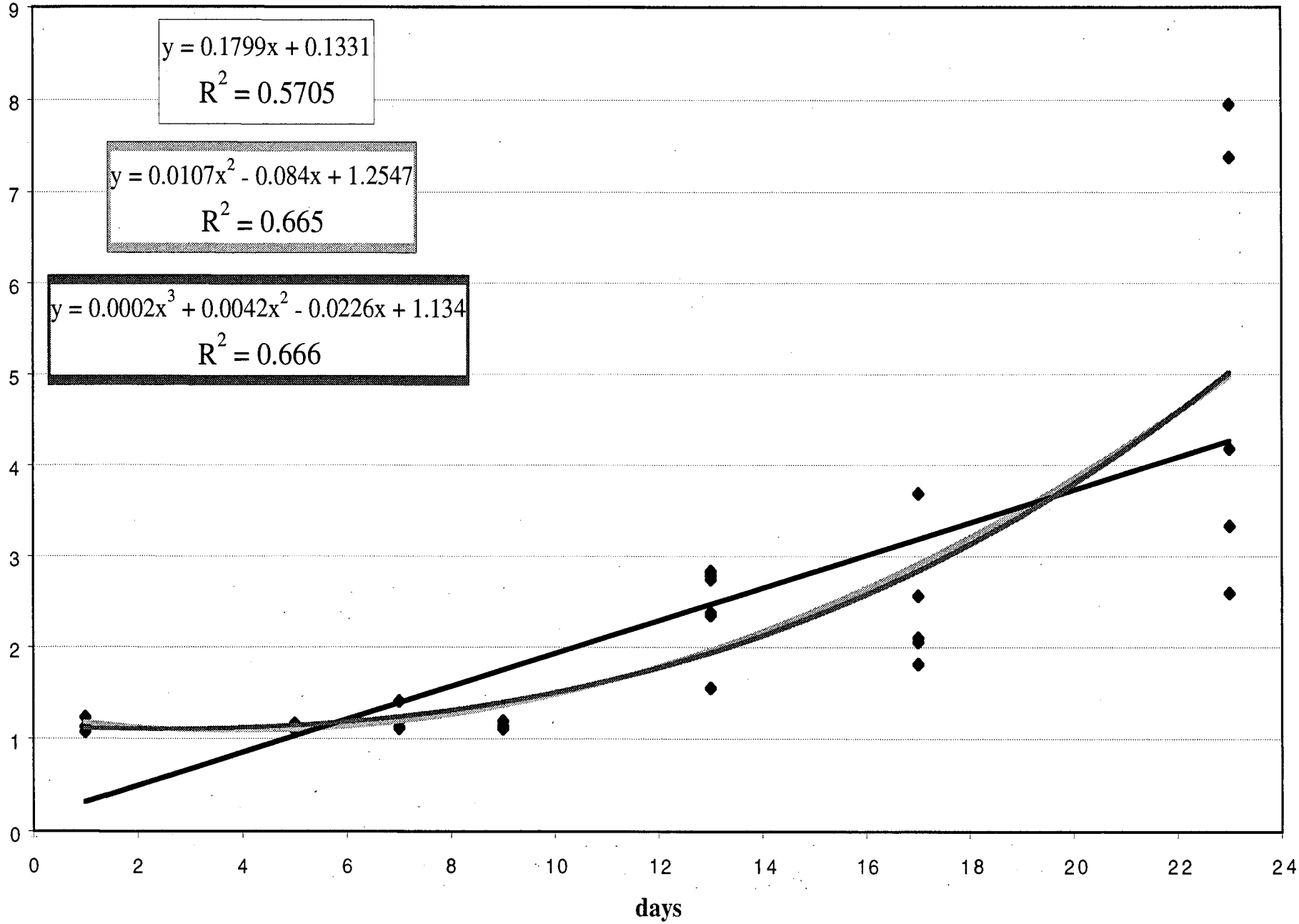

# Figure 7: Premaxillary/Frontal suture gender comparison

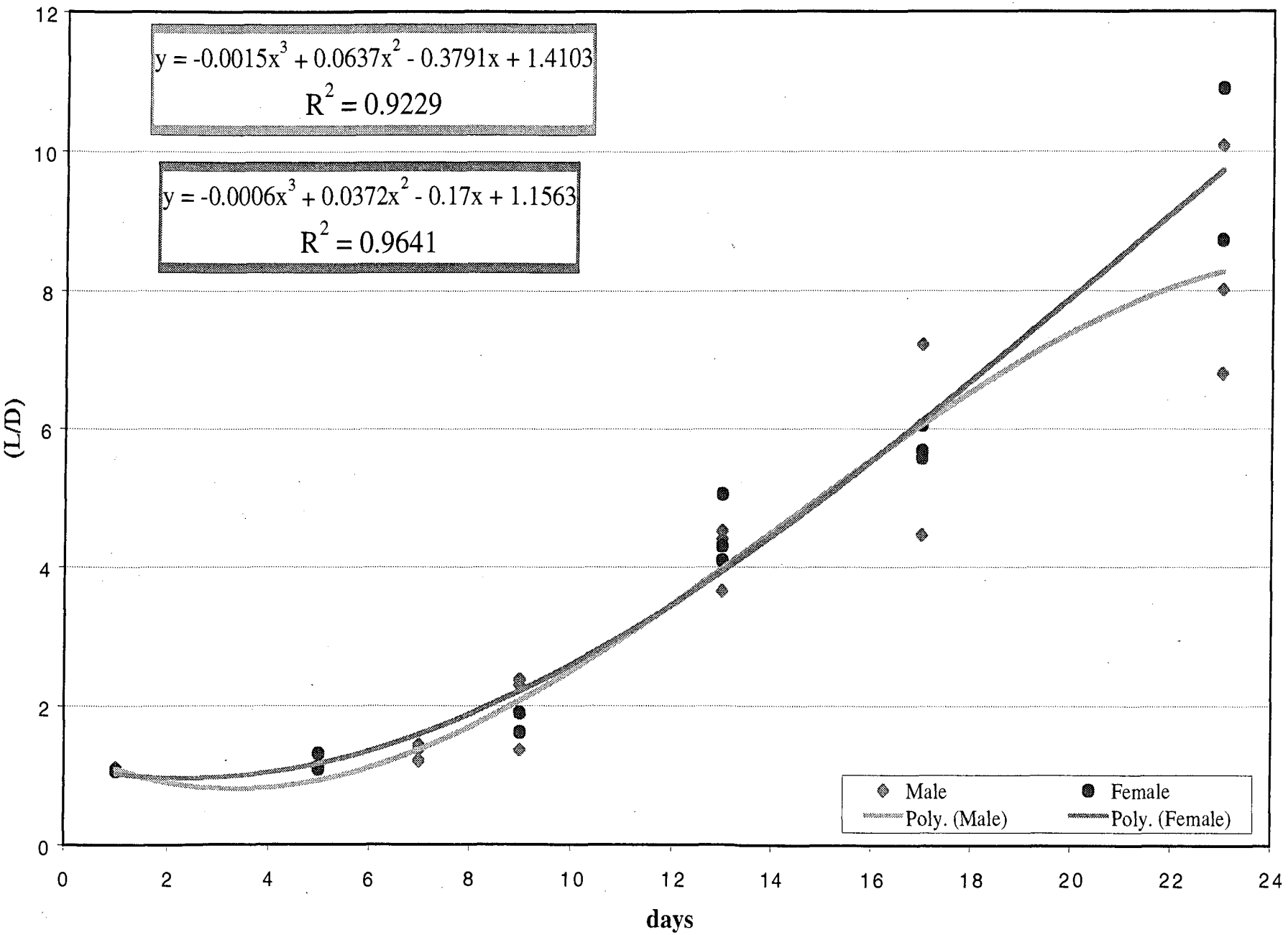

# Figure 8: Nasal/Frontal suture gender comparison

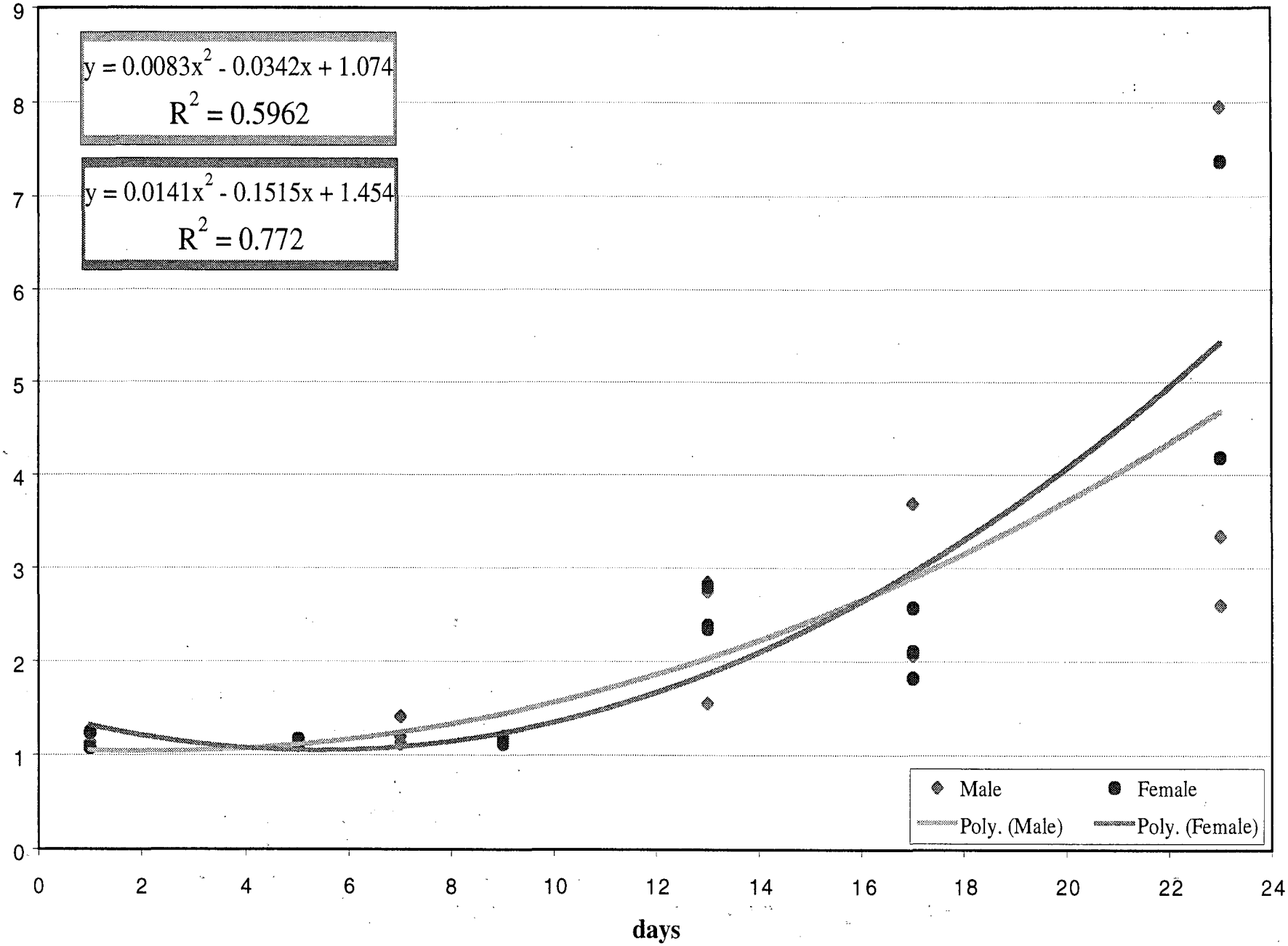

# Figure 9: PF/NF suture comparison v. time

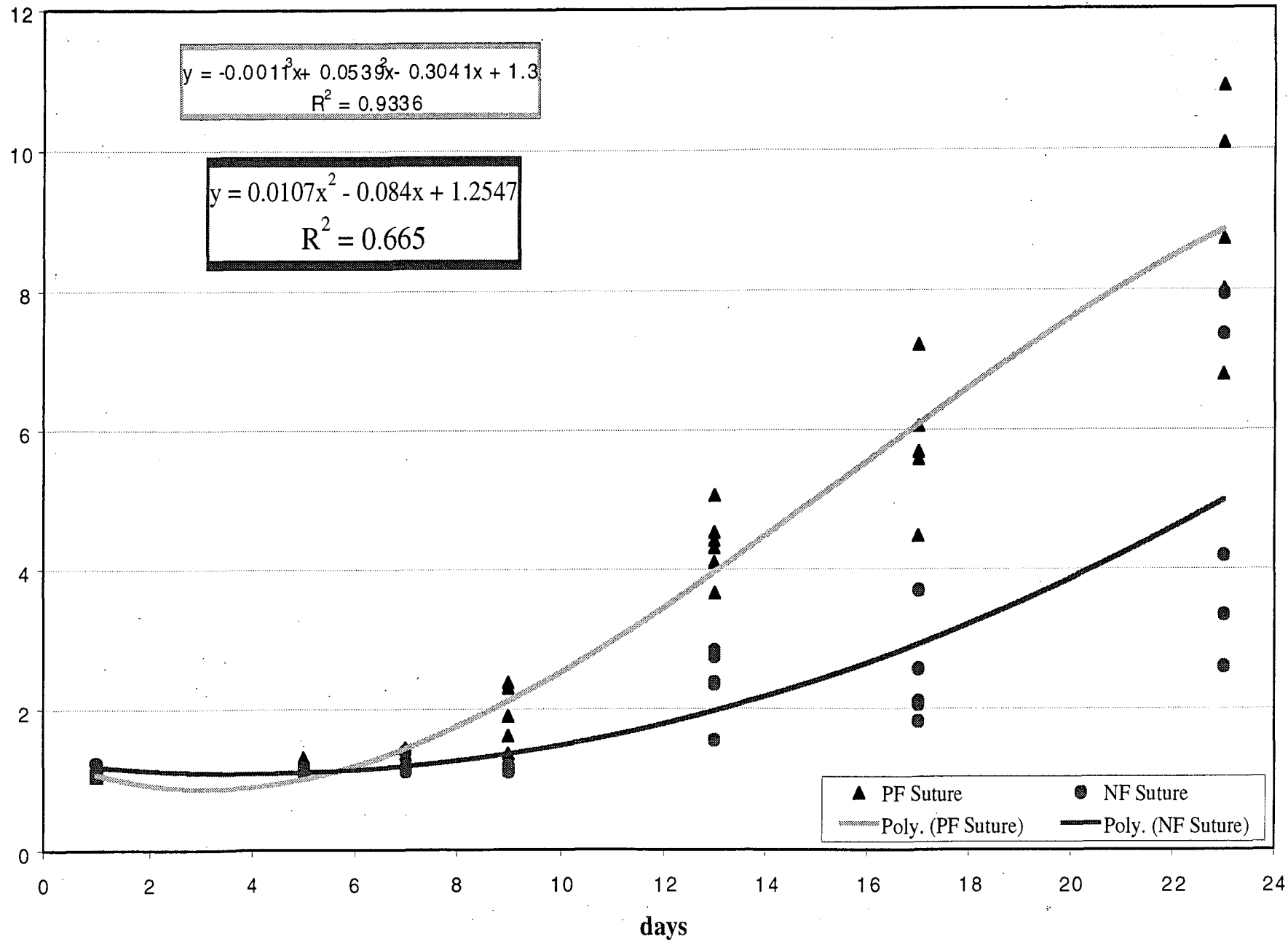

# Effects of Free Radical Decay on the UV-Vis-NIR Spectra of Irradiated Ultra-High Molecular Weight Polyethylene

James T Lyles, with M Shah Jahan

University Of Memphis, Tennessee, USA

**Abstract:**

The sterilization of medical grade ultra-high molecular weight polyethylene (UHMWPE) by gamma-irradiation causes the scission of the polymer chain, forming free radicals. The presence of free radicals in the polymer contributes to accelerated wear and premature failure of the implanted component.

For this study, thin film samples of UHMWPE were irradiated and then stored in either a nitrogen environment or in air at room temperature The UV-Vis-NIR spectrum of each sample was then studied over time.

The preliminary results of this study show that the reaction of free radicals in UHMWPE over time alter the absorbance of the spectrum in three regions; 240 nm, 1718 nm and 2300 nm. A larger body of data collected over a longer time period will be necessary to make any conclusive results.

## Introduction:

Joint arthroplasty is the surgical reconstruction of a damaged or diseased joint. The earliest arthroplasty preformed in the United States was an osteotomy of a hip joint and was preformed in Pennsylvania in 1826. The current method for performing an arthroplasty evolved from procedures developed by McKee, in 1951, and Charnley, in 1958. Since the development of these methods the trend has been to a total joint arthroplasty, as opposed to a hemiarthroplasty, or the partial replacement of a joint. As of 1962 the choice for the implant materials has been metal components that articulate on an ultra-high molecular weight polyethylene (UHMWPE) plate [1].

UHMWPE is a two-phase viscoplastic solid made of a series of crystalline domains in an amorphous matrix [1]. The crystalline regions are orthorhombic, monoclinic or hexagonal crystals in

folded rows making lamellae of 10-50 nm in thickness [1,2]. UHMWPE was chosen as the articulating surface due to its low coefficient of friction and biocompatibility. This biocompatibility is largely due to the large molecular weight of the polymer, over 4 million grams per mole [3].

Before an implant can be placed in the body it must be sterilized. Three methods of sterilization are currently employed: gas plasma sterilization, ethylene oxide gas sterilization, and gamma irradiation. Gamma irradiation is currently the most widely used method of sterilization, even though it produces free radicals in the polymer that can lead to premature failure of the implant [1, 3]. The formation of free radicals occurs when energy from the gamma radiation is transferred to the electrons in the polymer. These excited electrons transfer the extra energy thought the medium and break bonds in the polymer chain [4]. The various species that can form from the irradiation of UHMWPE can be seen in figure 1.

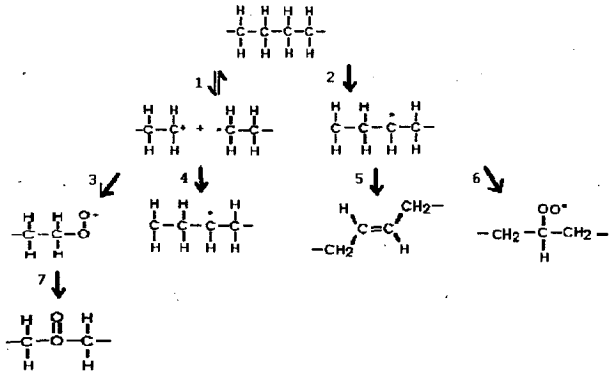

Fig. 1 Free radical reactions within UHMWPE

The UHMWPE can take one of two paths of free radical formation. The first, corresponding to reaction 1, is a breaking of the carbon-carbon bond. This break in the polymer chain is called a chain scission and forms a primary alkyl radical. If this scission occurs in the crystalline matrix, then the free radicals may recombine to form UHMWPE. However, if the primary alkyl radical continues to react it can take a hydrogen from an UHMWPE forming a secondary alkyl radical and a terminal polymer chain, reaction 4. If the primary alkyl radical comes into contact with oxygen then it can form a primary peroxy radical, reaction 3, which can further react to create a peroxide molecule, reaction 7.

If the scission of the UHMWPE occurs between a carbon-hydrogen bond then this is a branch

scission and follows reaction 2. The product of reaction 2 is a secondary alkyl radical, which by reaction 5 can rearrange and form an unsaturated trans-vinylene chain. If the secondary alkyl radical reacts with oxygen then it produces a secondary peroxy radical by reaction 6. This peroxy radical can react further to produce other species, such as ketones [5].

The radicals are known to be present in the polymer after irradiation from other studies. Both electron spin resonance (ESR) and Fourier transform infrared spectrometry (FT-IR) confirm the presence of the free radical species [6]. The purpose of this study was to evaluate the viability of using UV-Vis-NIR spectroscopy to identify the presence of free radicals in irradiated UHMWPE.

**Methods and Materials:**

The UHMWPE studied was UHMWPE 4150 manufactured by Smith & Nephew in Memphis, TN. An American Instruments, Inc. X-ray machine with a Molybdenum target, operated at 50 kV and 30 mA, was used to irradiate the UHMWPE. While a Varian Cary 5E UV-Vis-NIR Spectrometer was employed to record the spectra of the samples, which were mounted on the Varian solid film sample holder with an aperture of 5mm.

The bulk UHMWPE was cut into thin films with a thickness of either 140 microns or 200 microns. The film was then cut into rectangular samples about 10mm by 12mm. Each sample was marked in order to assure proper orientation in the sample holder.

Next, the spectrum of each sample prior to irradiation was recorded. The absorbance from 3200 nm to 200 nm was taken in an inert nitrogen chamber at room temperature, using a baseline correction zeroed to an empty sample holder in the nitrogen environment. The spectral bandwidth was fixed at 1 nm across the entire scan. An empty sample holder was used as the reference for each sample. Then, two of the samples were irradiated using 4 Mrad of X-ray irradiation for one hour. The spectrum of each irradiated sample was again taken immediately after the exposure to radiation using the same procedure. One sample was then stored in a nitrogen environment, while the other was placed in an air environment. The unirradiated sample was stored in air. All three samples were kept at room temperature. The spectrum of each sample was taken every half-hour for the first two hours and then daily for the next several weeks, using the same procedure as above.

**Results:**

The results of recording the spectrum of the 200 micron sample over 10 days yielded 3 regions where the absorbance changed for the irradiated sample stored in air and no change for the nitrogen stored or the unirradiated sample. The regions where an absorbance change was observed are: 240 nm, 1718 nm and 2300 nm.

The absorbance at 240 nm increases over time, as can be seen in figure 2. This increase was expected, since the irradiated UHMWPE can be seen, without the aid of any instrumentation, to darken over time in air. This increase suggests the development of a new species. However for any analysis to take place this peak must be resolved more clearly.

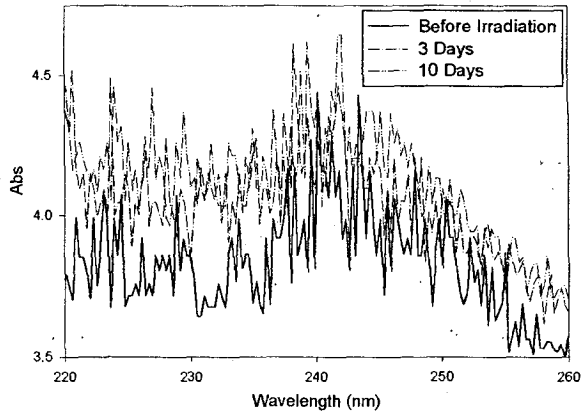


Fig. 2 Absorbance at 240 nm for irradiated air stored sample

The absorbance change at the 1718 nm peak for the air-stored sample can be seen in figure 3. The trend is a decrease in the absorbance over time, suggesting a decay of the radical species.

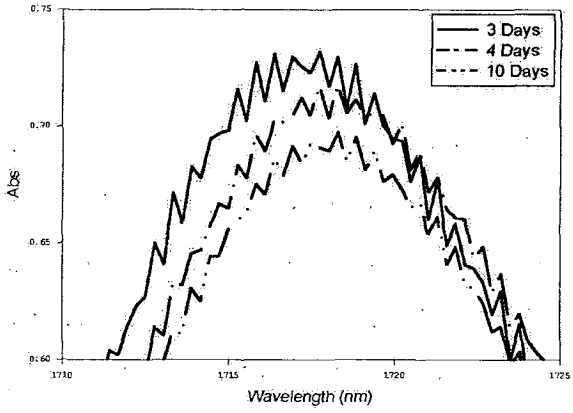


Fig. 3 Absorbance at 1718 nm for irradiated air stored sample

Just like the peak at 1718 nm the trend of the absorbance at 2300 nm is a decrease over time. This trend can be seen in figure 4 and again suggests the decay of a species over time.

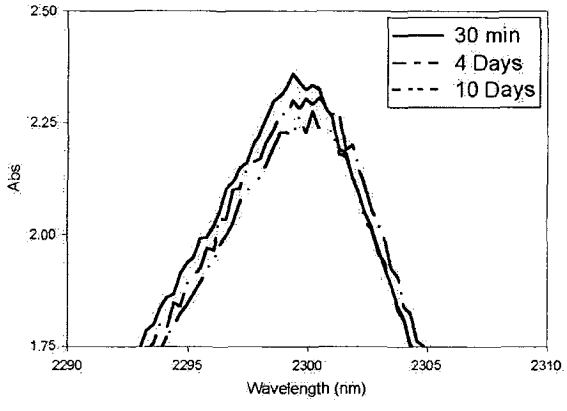


Fig. 4 Absorbance at 2300 nm for the irradiated air stored sample

The results of this study have been promising. However, further study will be necessary in order to establish UV-Vs-NIR spectroscopy as a method of free radical analysis for irradiated UHMWPE. Further data needs to be collected on the samples used in this study in order to ascertain if the trends seen thus far will continue. Also, the species responsible for these absorbencies need to be identified in order to make this a truly useful method of analysis.

**Acknowledgements:**

I would like to thank Smith & Nephew, Inc. for providing the samples that were studied. Also, I must thank the Physics Department at the University of Memphis for providing the equipment and facilities to undertake this research. The Biomedical Engineering Department at the University of Memphis must be thanked for organizing this Research Experiences for Undergraduates (REU) program. Lastly, I would like to thank the NSF for providing funding and making this research possible.

## References

[1] Kurtz SM, Muratoglu OK, Evans M, Edidin AA. Advances in the processing, sterilization, and crosslinking of ultra-high molecular weight polyethylene for total joint arthroplasty. Biomaterials 1999;20:1659-1688.

[2] Aggarwal, SL. Physical Constants of Polyethylene. In: Brandrup J, Immergut EH. Polymer Handbook. New York: Interscience Publisher, 1967: VI41-VI51.

[3] Kennedy FE, Currier JH, Plumet S, et al. Contact Fatigue of Ultra-High Molecular Weight Polyethylene Bearing Components of Knee Prostheses. J. Tribology 2000;122:332-339.

[4] Buchanan FJ, Sim B, Downes S. Influence of packaging conditions on the properties of gamma-irradiated UHMWPE following accelerated ageing and shelf ageing. Biomaterials 1999,20:823-837.

[5] Costa L, Luda MP, Trossarelli L, Brach del Prever EM, Crova M, Gallinaro P. Oxidation in orthopaedic UHMWPE sterilized by gamma-radiation and ethylene oxide. Biomaterials 1998,19:659-668.

[6] Goldman M, Lee M, Gronsky R, Pruitt L. Oxidation of ultrahigh molecular weight polyethylene characterized by Fourier Transform Infrared Spectrometry. J Biomed Mater Res 1997,37:43-50.

# Establishment of a Murine Model for Cisplatin-Induced Acute Ototoxicity

John W. Goss[1,2], Mark N. Kirstein[2], Maryam Fouladi[3], Jian Zuo[4], Clinton F. Stewart[2]
[1] Department of Biology, Rhodes College, Memphis, TN
[2] Department of Pharmaceutical Sciences, St. Jude Children's Research Hospital, Memphis, TN
[3] Department of Hematology/Oncology, St. Jude Children's Research Hospital, Memphis, TN
[4] Department of Developmental Neurobiology, St. Jude Children's Research Hospital, Memphis, TN

**Abstract:**

Cisplatin (CDDP) is an anti-cancer drug used in the treatment of children with medulloblastoma. However, dose-limiting ototoxicity has been observed in previous studies. The ototoxicity is caused by damage to the ciliary hair cells in the cochlea. The early damage that results from Cisplatin treatment is observed primarily in the regions of the cochlea sensitive to high frequency sounds (the basal region), and after time, damage is seen in the mid-basal and apical regions. For these studies, we used transgenic mice that possess a modified bacterial artificial chromosome (BAC) which contains a reporter gene that produces green fluorescence protein (GFP). Expression of this fluorescent protein allows us to easily view the ciliary hair cells within the cochlea using confocal microscopy. We administered varying doses of cisplatin to transgenic mice, and then observed the effects on the ciliary hair cells of the cochlea using confocal microscopy. By examining the damage, we attempted to derive a dose-response relationship. In addition, other regions of the cochlea (basal, first mid-basal, and second mid-basal) were examined to determine the relative damage between the regions resulting from cisplatin treatment.

## Introduction:

The anti-cancer drug cisplatin has proven effective in the treatment of a variety of solid tumors in adults and children. However, several side effects have been observed after cisplatin therapy including nephrotoxicity, neurotoxicity, ototoxicity, and gastrointestinal toxicity[1]. In children with medulloblastoma that were treated with cisplatin at St. Jude Children's Research Hospital on the protocol STM B96, ototoxicity was the dose-limiting toxicity. Studies have shown that cisplatin kills auditory neurons

and hair cells in the turns of the cochlea within the inner ear[1]. This cochlear cell and neuron destruction often begins in the cells that are most sensitive to higher sound frequencies. Because the audible ranges for humans are low frequencies, most of the patients are initially unaware that any hearing loss has occurred during cisplatin treatment; however, after three to six months, more profound hearing loss results as the damage is manifested[2].

Different frequencies of sound stimulate hair cells in different portions of the cochlea membrane in a gradient effect. In other words, different populations of hair cells respond to different frequencies of sound, depending upon their location within the cochlea (the basal, medial, and apical turns). The lower frequency sounds are best detected in the apical portion of the cochlea, while the higher frequencies of sound are best detected in the basal area[3]. A diagram of the cochlea in relation to the middle and outer ear is shown in **Figure 1**.

In order to recapitulate the condition of hearing loss observed in the clinic, we are using an animal model for cisplatin-induced hearing loss. For the purposes of this experiment, the basal area of the cochlea was examined to determine the amount of damage resulting from one-time treatments of cisplatin, since this site is often the area thought to be affected in children receiving cisplatin.

The mice used for these studies are transgenic mice developed by Dr. Jian Zuo that allow for special analysis of the ciliary hair cells within the cochlea. This murine model is particularly advantageous because the hair cells of the mice possess a modified bacterial artificial chromosome (BAC), which contains the reporter gene that produces green fluorescence protein. The green fluorescence protein gene in the transgenic mice allows us to easily view hair cell loss by confocal microscopy. This trait results in the living cochlear hair cells appearing bright green when viewed using confocal microscopy[4]. This method allows for quantitative analysis of the effects of cisplatin on those cells by determining a percentage of hair cell loss at each of the dosages. In addition, the amount of relative damage in the basal, first mid-basal, and second mid-basal regions of the cochlea can be observed using techniques described in Methods and Materials.

There are several disadvantages to using this murine model, however. First, the murine cochlea is very small, and thus very hard to dissect out and examine. Because the microdissection process is very difficult with the microscopic cochlea, it is very easy to damage the fragile ciliary hair cells within the cochlea turns. In addition, studies using the murine model for hearing loss are limited in the literature, since most investigations have been traditionally performed with larger animals such as gerbils or guinea pigs. Therefore, dosages of Cisplatin from prior experiments with gerbils and guinea pigs were used for this experiment in order to determine a maximum tolerable dose.

The goal of these studies is to develop a model for cisplatin-induced ototoxicity. We will first determine the maximum tolerated dose of cisplatin in mice. By this approach, we will maximize the amount of hair cell loss and develop a cisplatin dose-response relationship.

The development of this model has four main steps, which are genotyping for the presence of the green fluorescent protein gene (GFP(+)), administration of cisplatin to GFP(+) mice, cochlear dissection, and observation of hair cells using confocal microscopy.

**Methods and Materials :**

*Polymerase Chain Reaction Conditions*

In order to test for the presence of GFP, the Polymerase Chain Reaction (PCR) and gel electrophoresis procedures will be used. First, mice are anesthetized using isofluorane, and tail clippings are harvested. Tail clipping are treated with proteinase-K in a tail buffer solution (100mM Tris pH 8.0, 5mM EDTA, 0.2% SDS, and 200mM NaCl). Proteinase-K degrades tail material composed mainly of protein and the DNA remains intact. This DNA is then isolated within the solution using a centrifuge (13,600 rpm for 5 minutes) and the supernatant is poured into 600 uL of isopropanol. This solution is centrifuged under the same conditions, and the liquid decanted. The remaining pellet of DNA is washed with 300 uL of 70% Ethanol, dried for 30 minutes, and then suspended in 200 uL of water. Next, 1 uL of each sample of DNA solution was mixed with 19.65 uL deionized water, 2.5 uL of $MgCl_2$ buffer solution, 1.25 uL of dNTP

solution of base pairs, 0.75 uL of each of the primers in the set of primers A9B3/EGFRL-1 and BACL-F/ BACL-R (for a total of 1.5 uL of primer in each mixture), and 0.1 uL of Taq polymerase. A diagram of this mixture is shown in **Figure 2**. This mixture is then loaded into the PCR apparatus (MJ Research; Watertown, Massachusetts) for replication of the relevant DNA.

The PCR process for the DNA samples occurs in three main stages, which are repeated many times in order to amplify the relevant DNA for analysis. First, the double helix of the DNA strands are denatured at 94°C resulting in formation of single stranded templates. The temperature is then decreased to 54°C, allowing for the primers to pair with the resultant single stranded template by ionic bonds. After approximately 45 seconds has passed (which is enough time to allow for this strong ionic bond to form) the temperature is increased to 72°C, which allows the Taq polymerase to promote chain extension by adding base pairs to the template strand. Complementary bases are then bonded throughout the length of the template, eventually forming a DNA strand that is complementary to the original template[5]. A diagram of the procedure is shown in **Figure 3**. This entire process (one cycle) takes approximately 4 minutes. In this procedure, thirty-five cycles are run in order to get an amount of DNA sufficient for viewing by gel electrophoresis.

After the PCR reaction is complete, 20 uL of each of the product DNA samples are mixed with 5 uL of the loading buffer Load B 2KB (composed of 30% glycerol in water and 25% xylene cyanol), and they are loaded into individual wells of a 1.2% agarose electrophoretic gel. Positive and negative controls for the GFP gene are also used to allow identification of positive lanes. Then, a current of 150 volts was run through the gel to separate out the genes within the sample. After one hour, the gel was removed from the current and exposed to UV light in order to view the DNA fragments, and to photograph it. By analyzing the picture, the presence or absence of the GFP character is easily determined in each of the tail DNA samples. The mice corresponding with positive GFP expression can then be used for the next phase of the experiment.

*Cisplatin Administration*

The second stage of the study is administration of cisplatin to the GFP positive mice. Cohorts of mice are given increasing cisplatin doses intraperitoneally in order to determine a dose-response relationship. In addition, a control mouse was injected with saline (which allows us to determine relative hair cell loss due to cisplatin). The mouse identified as CDDP 26 was treated with a 14 mg/Kg dose of Cisplatin (333 uL), and the mouse identified as CDDP 31 was treated with a 16 mg/Kg dose of Cisplatin (243 uL). The mouse identified as CDDP 30 was used as the control for this experiment.

*Cochlear Dissection*

After three days, the mice are sacrificed, and perfused with 4% PFA, after which time the cochlea are dissected to observe the effects of the drug. To remove the cochlea, the mouse the mice are perfused with 4% PFA in a phosphate buffer solution, in order to purge the blood away from the organs and decrease background interference. Mice are decapitated and the petrosal region is isolated from the other structures through gross scale dissection. This segment is then soaked in 150 mM of EDTA at 4°C for seven to ten days. The EDTA softens the bone and tissue surrounding the cochlea, which allows for easier removal using microdissection techniques.

After seven to ten days of EDTA incubation, the cochlea are then microdissected using a dissecting microscope and micro-dissection tools. The cochlea is first separated from the rest of the tissue and bone material surrounding it (including the semi-circular canal).

A preliminary cut followed by three major cuts was made to prepare the cochlea for viewing under the confocal microscope (as depicted in **Figure 4**). The preliminary cut is made just below the round windows, and it separates the cochlea from the semicircular canal. The first major cut (labeled cut 1 in Figure 4) is made at the base of the cochlea. This cut isolates the basal turn of the cochlea from the rest of the cochlea body. This segment of the cochlea is labeled (1) in **Figure 4**. Next the remaining portion of the cochlea body is cut down the middle into halves (cut 2 in Figure 4). These portions are labeled (2) and (4) on one half and (3) and (5) on the other half. Finally, the cochlea is viewed in a saggital plane (as seen in **Figure 5**) and the nerves that connect sections (2) and (4) (and sections (3) and (5) on the other half) are severed (cut 3 in

Figure 4), which allow the two halves to be separated without tearing them. After clearing away some of the excess bone and tissue, the ciliary hair cells are then visible along each of the cochlea turns.

*Confocal Microscopy*

Confocal microscopy is used to view the GFP expression in cochlear cells. In this form of microscopy, photographs of the slide are taken in several planes, and the images are then combined to form a three-dimensional image along the z-axis. By using this method of microscopy, the effects of cisplatin administration on the ciliary hair cells can be better quantitated through determining a percentage of damaged cells.

Each of the cochlear regions are placed onto a hanging-drop slide, and immersed in four to five drops of Fluromount-G (which serves as a semi-permanent seal). A glass coverslip is then placed over the slide, and each of the cochlear regions are viewed using the confocal microscope at 20X magnification. The ciliary hair cells from the basal region are first observed to determine the damage present. Finally, the ciliary cells of the first and second mid-basal regions of the cochlea are observed using confocal microscopy in order to determine the damage present in each of them.

**Results:**

After carrying out the PCR procedure, the mice identified as CDDP 26, CDDP 30, CDDP 31 were determined to be GFP(+). The electrophoresis gel shown in **Figure 6** shows the expression of the GFP trait in those mice. Two of these GFP(+) mice were used for cisplatin administration and the other GFP(+) mouse was used as a control animal.

After the administration of cisplatin, the isolated basal, first mid-basal, and second mid-basal regions of the cochlea were viewed using confocal microscopy. The regions labeled (1) through (5) are the basal region, the first mid-basal region, the second mid-basal region, the first apical region, and the second apical region, respectively. A diagram of each of these regions is shown in **Figure 4**.

The first area examined was the basal region of the cochlea. However, the hair cells of this region could not be observed due to mechanical damage during micro-

dissection and high levels of background interference. Therefore, the first mid-basal region of the cochlea was then examined, and the ciliary hair cells could be observed in this area. **Figure 7A** shows an image taken by the confocal microscope of ciliary hair cells of the first mid-basal region from the left ear of the mouse identified as CDDP 26. Not much detail can be seen from this picture, but the three rows of hair cells can be seen at the periphery of the tissue. The bright fluorescent portions that stand out from the rest of the green tissue are the ciliary hair cells. Damaged cells are indicated by dark gaps between these bright fluorescent cells. **Figure 7C** (the right ear of CDDP 26), **Figure 7D** (the left ear of CDDP 31), and **Figure 7G** (the left ear of CDDP 30) also show the ciliary hair cells of the first mid-basal region. However, the individual hair cells can not be clearly identified in these images due to background interference. The damaged cells in the first mid-basal region could not be quantified based on these images of the ciliary hair cells.

The second mid-basal regions were then examined. The ciliary hair cells of this region were more visible than in the first mid-basal region. **Figure 7B** (the left ear of CDDP 26) and **Figure 7F** (the right ear of CDDP 31) show the three rows of hair cells quite clearly. However, **Figure 7E** (the left ear of CDDP 31) and **Figure 7H** (the left ear of CDDP 30) have a large amount of background interference, and the individual hair cells can not be identified. The individual ciliary hair cells are slightly more visible in this region, but the images are not clear enough for an accurate quantitative analysis of the damaged cells.

**Discussion:**

After the mice identified as CDDP 26, CDDP 30, and CDDP 31 were determined to be GFP(+) by the polymerase chain reaction procedure, cisplatin was administered. A dose of 14 mg/Kg was administered to CDDP 26, 16 mg/Kg was administered to CDDP 31, and CDDP 30 was used as the control mouse.

The basal region of each of the cochlea was then micro-dissected and examined using confocal microscopy. However, the ciliary hair cells from this region could not be seen. We were unable to get a clear picture of the cochlear basal region upon examination with the confocal microscope for two main reasons. The first of these is the difficulty in

the micro-dissection process. Because the murine cochlea is so small, it is very difficult to isolate the separate regions, while not damaging the ciliary hair cells. The lack of clarity in not only the basal cochlear region, but also the other regions could also be the result of the cochlea being soaked for too long in the 4% PFA solution. It is possible that this resulted in a high degree of background interference making the hair cells less visible under the confocal microscope. In the future, the cochlea should be kept in the 4% PFA for a shorter period of time in case this prolonged soaking is responsible for the background interference. In addition, it has been hypothesized that those cohorts in which there is little contrast between the background tissues and the ciliary hair cells are heterozygotes for the GFP trait. It is thought that in these individuals the green fluorescence of the ciliary hair cells is not as bright and, therefore, they do not stand out quite as much.

The first and second mid-basal regions of the cochlea were then examined from the cochlea of each of the three mice. The images of the first mid-basal region show the ciliary hair cells, but the clarity of the image is poor for the same reasons described above. Because the individual ciliary hair cells could not be differentiated from one another, no quantitative analysis of the damage in the first mid-basal region resulting from cisplatin treatment could be conducted. However, there appear to be very few dark gaps that stand out, leading me to conclude that the cisplatin doses administered in this experiment resulted in minimal hair cell damage.

The images of the second mid-basal region show the ciliary hair cells more clearly than in the basal or first mid-basal regions, however the clarity of some images is still poor, once again due to the reasons described above. The individual ciliary hair cells could be somewhat identified in left ear of the cisplatin treated mouse CDDP 26 (**Figure 7B**) and the right ear of the cisplatin treated mouse CDDP 31 (**Figure 7F**), but those in the left ear of the control mouse CDDP 30 (**Figure 7H**) could not been identified. The images are not quite clear enough for an accurate analysis of the ciliary hair cells quantitatively, but in the left ear of CDDP 26 it appears only six hair cells within the viewed region are damaged. In the right ear of CDDP 31, it appears that only one hair cell within the viewed region is damaged. Both of these damage levels appear to be

minimal, but because the images from the control mouse were unclear, a true comparison between the two dosages can not be made.

Based on the results of this experiment, no conclusions could be drawn about a dose-response relationship between cisplatin and ciliary hair cell damage. For doses of 14 mg/Kg and 16 mg/Kg very little hair cell damage was observed. In addition, the lack of image clarity prevented a comparison of damage in the basal, first mid-basal, and second mid-basal regions of the cochlea.

It is likely that administering higher dosages of cisplatin could result in a more accurate dose-response relationship. Because little hair cell damage was observed at 14mg/Kg and 16mg/Kg, higher doses could give more information regarding the dose-response relationship between cisplatin and ciliary hair cell damage. It is also possible that a change in the method of dosage could lead to more accurate results. While the parameters of this experiment can give a model for the dose-response relationship of cisplatin, it is uncertain how closely these results actually recapitulate the conditions observed in the clinical setting. In this experiment, the cisplatin was administered in single, varying doses and the effects were observed afterwards. However, in the clinical setting, several doses of cisplatin are given at regular intervals over much longer periods of time. So the dose-response relationship determined from the single administration of cisplatin in this experiments may not actually reflect the cochlea damage that occurs with continuous treatment over a long period of time.

By continuing to test the ototoxicity of varying doses of cisplatin on mice, an accurate dose-response model of cisplatin-induced hair cell loss can be established. This model can then be used in the later stages of this project to test the potential for otoprotection by Amifostine administration, given along with cisplatin, on the cochlea ciliary hair cells. If amifostine is an effective otoprotective drug, then its effects can be quantitatively observed when it is administered with cisplatin in the transgenic mouse model. If more living cilia (those that are fluorescent green) are observed after treatment, then the amifostine has prevented some of the ototoxic effect of the cisplatin. In addition, this model can be used to quantitatively compare the effects of different dosages of amifostine on the cisplatin treated transgenic mouse model.

**Figures Legend**

## References


1. Smooreburg GF, DeGrost JC, Hamers FP, and Klis SF. (1999) *Ann NY Acad.Sci.* 884, 192-210.
2. Liberman, M. Charles. (1990) *Toxicology Pathology* 18, 138-148.
3. Kelly, James P. Principles of Neuroscience, 3rd Edition, Kandel, Schwartz, and Jessell.
4. Zuo J, Treadway J, Buckner T, Fritzsch B. (1999) PNAS 96, 14100-14105
5. Principle of PCR. Microsoft Explorer. 23 October 2000

# Isolation of Mutants of *Aspergillus nidulans* Showing Hypersensitivity to Calcofluor White

Amit Mirchandani, Jennifer Livesay, Mridula Bagrodia

## Introduction:

Fungi are pervasive, abundant and important organisms, found throughout the globe from the microscopic to the macroscopic world. Found as food, as mold on food, in medications, and as the cause of various plant and animal diseases, virtually every person has come into contact with these ubiquitous microorganisms. Considering this, it is easy to see how the oft-unnoticed influence of fungi on human activity makes it important to study these organisms. Although there is great diversity and variety among the microorganisms of the Kingdom Fungi, several general characterizations can be made. Fungi are eukaryotic organisms, whose primary organizational structure is at the cellular level. Other common characteristics are reproduction through sporulation, branched filamentous cells (hyphae), and the fact that all fungal cells possess a cell wall (Moore-Landecker, 1996).

The cell wall provides support and protection for the fungus, and it must be rigid enough to fulfill this function while simultaneously being flexible enough to allow for hyphal branching or cell growth. The main skeletal framework of the fungal cell wall consists of the chitin polymers. These fibrillar polysaccharides are embedded in matrix polymers, such as glucans, which are components of the cell wall. Also present are proteins, some of which may play structural roles, while others are involved in the synthesis or developmental modifications of the structural polymers (Gow and Gadd, 1995).

As is the case with all complex cellular processes the role of proteins in regulation is critical. The best way to investigate role of proteins in the cell wall is to alter genes involved in cell wall metabolism. It is imperative that we understand the genetic sphere of cell wall synthesis in order to specify the proteins involved in cell wall metabolism.

Our work this term has been to investigate cell wall metabolism in the fungus *Aspergillus nidulans*. The ultimate goal of cell wall research of *A. nidulans* is to expand the number of genes known to code for proteins involved in cell wall synthesis. In order to do so, we must start with a limited number of mutant alleles and determine the chromosomal location of these genes and these alleles are dominant or recessive in what they code for. Our current research goals will enable us to obtain the

"genetic tools" needed to further our understanding of cell wall metabolism from a basic genetic perspective. This entails isolating genetic mutants causing a wide range of defects in cell wall assembly and specifically identifying the defect. The research conducted to date is only a fraction of the ultimate goal, yet it is essential in order for research to advance.

**Methods:**

In order to identify genetically mutated colonies with respect to cell wall synthesis, a collection of chemically mutagenized strains was screened for hypersensitivity to Calcofluor (CFW), a chemical that interferes with chitin fibril formation during cell wall assembly. This screening identified an initial set of 52 CFW-hypersensitive strains. Eighteen mutant strains from the initial mutant collection were chosen and mated with a CFW(-) resistant strain (AH 12) on minimal medium (MM), using complementary auxotrophy to select for heterokaryons (Table 1).

**Table 1. Mutant Strains**

| | | | |
|---|---|---|---|
| 1-18 | 2-99 | 2-453 | 8-3 |
| 1-48 | 2-179 | 6-6 | 8-125 |
| 1-49 | 2-202 | 6-107 | 10-148 |
| 1-161 | 2-217 | 7-13 | 12-40 |

All mutants were arginine plus (Arg+), PABA minus (PABA –), meaning they have the ability to synthesize arginine, but not paraaminobenzoic acid), while AH12 is PABA(+) and Arg (-), thus incapable of synthesizing arginine its own. Cleistothecia were isolated after 3 weeks growth on minimal medium, and ascospores representing the haploid progeny of the mating were germinated on complete medium plates. Approximately 100 resulting colonies from each cross were tested for CFW sensitivity and auxotrophic pattern. The protocol employed the same methodology for testing CFW as Momany, *et. al.* (1999).

**Results:**

Phenotypic ratios (CFW Sensitive: CFW Resistant) were determined, shown in Table 2.

**Table 2: Results from the First 16 Mutants**

| Mutant Strain | Ratio (S:R) | Mendelian Ratio |
|---|---|---|
| 1-18 | 47:53 | 1:1 |
| 1-48 | 45:55 | 1:1 |
| 1-49 | 39:43 | 1:1 |
| 1-161 | 48:52 | 1:1 |
| 2-99 | 57:42 | 1:1 |
| 2-179 | 71:29 | 3:1 |
| 2-202 | 49:51 | 1:1 |
| 2-217 | 47:53 | 1:1 |
| 2-453 | 37:63 | ??? |
| 6-6 | 52:47 | 1:1 |
| 6-107 | 49:51 | 1:1 |
| 7-13 | 29:71 | 1:3 |
| 8-3 | 77:23 | 3:1 |
| 8-125 | 72:28 | 3:1 |
| 10-148 | 37:63 | ??? |
| 12:40 | 42:58 | 1:1 |

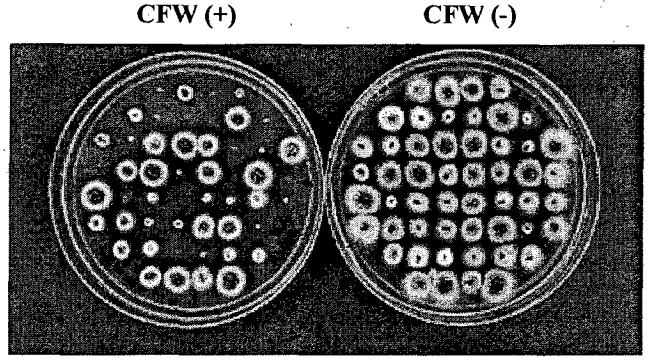


**Figure 1. Colonies of progeny from a cross between 1-49 and AH12 +/- Sub-lethal Levels of Calcofluor**

***Note that the mutant strains have reduced growth in the presence of the wall synthesis inhibitor.***

In our research investigating the genes that control cell wall synthesis, we first focused on mutant strains where only one damaged gene was found to be involved in building the mutant's cell wall. We were able to identify 10 mutants that displayed the 1:1 phenotypic ratio expected of single gene mutations [Figure 1]. In addition, there were three mutants whose crosses resulted in a 3:1 ratio, which suggest that two genes are responsible for the phenotype of these mutants. These results led to three independent lines of further investigation.

**Project 1 (Jennifer Livesay)**

Later steps in the characterization of these mutants will require strains exhibiting the mutant phenotype in combination with different combinations of auxotrophic markers and, ideally, different spore color markers as well. In many of the original 18 crosses, some expected phenotypes were not found. Therefore, this project searched the expression of specific phenotypes and auxotrophies for each of the 7 different crosses examined (1-18, 1-48, 2-99, 2-179, 2-202, 6-107, 8-25), as shown in Table 3.

**Table 3 : Results From Project 2: Investigating Specific CFW Sensitive Mutants**

| Mutant strain | Desired *arg* auxotrophy | Desired PABA auxotroph | Desired color | Observered |
|---|---|---|---|---|
| 1-18 | (-) | (+) | green and chartreuse | yes - both |
| 1-48 | (-) | (+) | green | no |
| 2-99 | (+) | (-) | green or chartreuse | no |
| 2-179 | (+) | (-) | green or chartreuse | no |
| 2-202 | (+) | (-) | green or chartreuse | no |
| 6-107 | (+) | (-) | green or chartreuse | no |
| 8-25 | (+) | (-) | green or chartreuse | no |

The colonies from these crosses were transferred to MM + Arg, MM + PABA and MM + Arg + PABA plates. Colonies that grew on MM + Arg and MM + Arg + PABA, but not on MM + PABA are ones that cannot manufacture the arginine on their own. The auxotrophic combinations needed were green or chartreuse Arg (+)/PABA(-) CFW sensitive individuals for mutants for 2-99, 2-179, 2-202, 6-107, and 8-25. No individuals were found for these mutants with this combination of auxotrophies. This leads to speculation about possible linkages. The other needed auxotrophic combinations were green or chartreuse Arg(-)/PABA(+) CFW sensitives for mutants 1-18 and 1-48. The only sought-after

combination found were one green and one chartreuse 1-18 (Arg(-)/ PABA(+). These colonies were originally brown on complete medium + Arg but showed distinct color tincture when grown on the MM + Arg and MM + PABA plates. No other colored mutants of this auxotrophic combination were found.

**Project 2 (Amit Mirchandani)**

This project addressed the possibility of gene linkage. In Mutant 2-453, all 100 of our CFW sensitive colonies were Arg(+) and either PABA (+) or PABA (-). Thus, we concluded that Arg(+) and CFW sensitivity traits are closely linked at the *arg*B locus for mutant 2-453. This project served to find a colony, which was both sensitive to CFW and Arg (-) and PABA (+). Since this colony had not been found yet, we looked further at a much larger number of colonies, and eventually found 5 out of 150. We tested these 5 colonies of mutant 2-453 on MM + PABA, and MM + Arg + PABA, we hoped to find the variant colony by identifying a colony which grows on MM + Arg and MM + Arg + PABA, but NOT on MM + PABA. After testing 150 CFW sensitive colonies, we found three colonies that fit our criteria.

**Project 3 (Mridula Bagrodia)**

The last project addressed the 3:1 Mendelian ratio of CFW Sensitive to CFW resistant colonies in the mutant strain, 2-179. Upon closer observation, it was ascertained that the ratio could also be interpreted as a 2:1:1, in terms of supersensitive (no germination in the presence of CFW), sensitive (little or altered growth in presence of CFW), and Resistant (normal growth in presence of CFW). One possible explanation is that perhaps this mutant has 2 genes contributing to CFW hypersensitivity: one in which there is a sensitive resistive phenotype and the other where there is a recessive super sensitive phenotype. To investigate this possibility, we backcrossed several Arg (+), PABA (-), and supersensitive mutants to AH12 and examined the ratios of 100 tested colonies for each strain. Although the expected ratios were not observed, some strains did assort 1:1 and were set aside for further research.. The phenotypic ratios (CFW Sensitive: CFW Resistant) of the investigated mutant strains are shown in Table 4.

**Table 4: Results from Project 3: Further Investigation of Mutant 2-179 for 1:1 Ratios**

| Strain | Ratio (S:R) | 1:1 Assortment |
|---|---|---|
| 2-179: A30 | 59:39 | NO |
| 2-179: A37 | 56:42 | YES |
| 2-179: A49 | 53:43 | YES |
| 2-179: A33 | 55:33 | NO |
| 2-179: A7 | 37:61 | NO |
| 2-179: A47 | 49:45 | YES |

## Discussion

Isolation of cell wall mutants has been previously researched by Ram et al (1994), with respect to CFW Hypersensitivity. His group identified a variety of genes implicated in cell wall metabolism of yeast and this suggests that the method may be applicable to filamentous fungi like *A. nidulans* with similar success.. Upon conclusion of this semester's work, we have promising results. In addition to finding ten strains that exhibit a 1:1 ratio in regards to sensitivity to CFW, we have also widened our range of auxotrophic backgrounds for future matings. Furthermore, there is a strong indication that one strain (2-453) is closely linked to the *arg*B locus which has already been mapped. In project 2, merely 2.7% of the sensitive colonies were recombinant with regards to the *arg*B locus, which can be found on chromosome 3.[4] This finding puts us in position to begin cloning this particular gene.

All but one of our mutants (2-217) have since been successfully crossed and have been shown to belong to independent complementation groups (i.e. to be distinct genes). [5] Since we have not yet had two mutants in the same gene, we conclude that several genes are involved in the complicated and extensive process of cell wall assembly. Although we cannot make any firm predictions at this time, our knowledge of the genetic basis of cell wall synthesis has been broadened and new avenues of cell wall research can be explored.

## References


1.) Momany, Michelle, Westfall, Patrick J., and Abramowsky, Gretel., 1999. *Aspergillus nidulans swo* Mutants Show Defects in Polarity Establishment, Polarity Maintenance and Hyphal Morphogenesis. Genetics. **151**; 557-567.

2.) Moore-Landecker, Elizabeth, Fundamentals of the Fungi. 4th ed. London: Prentice-Hall Inc.1996, 1-17.

3.) Ram, Arthur F.J, Wolters, Aly, Ten Hoopen, Rogier, Klis, Frans M., et al., 1994. A New Approach for Isolating Cell Wall Mutants in *Saccharomyces cerevisiae* by Screening for Hypersensitivity to Calcofluor White. Yeast. **10**; 1019-1030.

4.) Berse, B. et al, 1983. Gene 25:109-117 compiled by John Clutterbuck, University of Glasgow. http://www.gla.ac.uk/ACAD/IBLS/molgn/aspergillus/locia.html

5.) Drs. Terry Hill and Darlene Loprete (Personal Communication)

6.) Gow, Neil and Gadd, Geoffrey M., The Growing Fungus. London: Chapman and Hall. 1995, 41-63.

# Non-Heme Macrophage Iron in the Kidney and Spleen of Teleost Fishes: Semi-Quantification Using Acid Ferrocyanide Reactivity Grading of Organ Imprint Preparations

Ellen H. Barton and James C. Barton, M.D.

*Department of Biology, Rhodes College, Memphis, Tennessee and Southern Iron Disorders Center, Birmingham, Alabama*

**Abstract:**

**Background:** Semi-quantification of macrophage-associated iron in kidneys and spleens of teleosts has required preparation and analysis of tissue sections.

**Materials and Methods:** Imprints of kidneys or spleens of 70 adult teleosts of 22 species were prepared, stained with acid ferrocyanide (AF) to visualize non-heme ferric iron (AF reactivity, AFR), and graded by light microscopy (AFRG).

**Results:** AFR was limited to macrophages. There was a significant positive correlation of AFRG values in 12 pairs of replicate imprint preparations. AFRG values in six pairs of imprint and tissue section preparations revealed a significant positive correlation. AFR was not detected in either organ in the channel catfish (Ictaluridae) or in the Carangidae. In the Serranidae, Lutjanidae, and Sparidae, intermediate mean AFRG values were obtained. AFRG values were greatest among the Scombridae, Ballistidae, and Pomadasyidae. Across 13 species, the correlation coefficient of AFRG values from paired kidney and spleen imprints from the same individuals was positive but not significant. When fish were grouped by taxonomic families, however, a comparison of mean AFRG of imprint preparations suggests that spleen AFR is greater than kidney AFR, on the average.

**Conclusions:**

The present method is a simple, replicable, and inexpensive technique by which relative quantities of non-heme ferric iron in kidneys or spleens of teleosts can be estimated and compared, and may be useful for the evaluation of disorders of iron metabolism.

**Introduction:**

In teleost fishes, iron homeostasis is maintained by controlled absorption of iron from food and ambient water (1, 2), macrophage recycling of hemoglobin-associated iron after phagocytosis of erythrocytes (erythrophagocytosis) (3, 4), and limited iron excretion (3, 5, 6). Thus, macrophage erythrophagocytosis (4, 7 - 9), iron-containing macrophages (8, 10 - 13), and relatively great concentrations of ferritin (14 - 16) occur in teleost kidneys and spleens. Previously described techniques of localizing and semi-quantifying macrophage iron in fish kidneys and spleens by light microscopy rely on visualization of non-heme ferric iron with acid ferrocyanide (AF) technique (Prussian blue reaction) (13, 17). In one method, AF reactivity (AFR) in melanomacrophage centers (MMC) is graded using a non-numeric scheme (13). In another, video image capture and computerized measurement of microscopic images are employed to quantify the area of AFR (17).

The purpose of the present study was to develop and validate a sensitive, rapid, and inexpensive method by which macrophage iron in fish kidneys and spleens can be visualized and semi-quantified for research or clinical purposes. The present method uses organ imprint preparations stained to visualize AFR and more explicitly defined, numerical histochemical grading criteria. Using the present method, we also evaluated kidney and spleen macrophage AFR in 22 species of teleosts, and compared the relative amounts of kidney and spleen macrophage AFR in fishes grouped by taxonomic families. The present results are discussed and compared with previously published observations of macrophages, erythrophagocytosis, macrophage iron, and normal and disordered iron metabolism in teleost fishes.

## Materials and Methods:

**Collection of Fish:** Pond-raised adult channel catfish (*Ictalurus punctatus* Rafinesque) were collected in April, and stunned by application of an electric shock to the water in their holding tank. Kidneys and spleens were removed through an abdominal incision, and the fish were then returned for commercial processing. Specimen preparation was completed within 10 minutes after organ removal. Wild, apparently healthy adult marine fish were caught using hook and line in the northern Gulf of Mexico within 20 miles of Destin, FL in October and November. Each fish was packed in ice immediately after its capture; kidneys and spleens were removed for study during routine preparation of the fish for human consumption. Initial specimen processing was completed within three hours after removal of each fish from water. Identification of each species was verified using a standard reference (18).

**Cytotechnique and Histotechnique:** *Preparation of imprint preparations.* Multiple imprints of kidneys or spleens were made on clean glass slides after section of the organs with a clean scalpel. Typically, imprints were applied approximately two-thirds of the slide area. Imprints for staining with AF technique were fixed in buffered formol acetone for 6 minutes (19). Additional imprints for Wright's/Giemsa staining were fixed as part of the staining sequence.

*Preparation of tissue sections.* Samples of kidneys or spleens from six species were fixed in neutral buffered formalin for 18 - 24 hours; duplicate specimens were fixed in buffered formol acetone for 18 - 24 hours (19). After automated paraffin embedding, 5 μm sections from each block were routinely prepared using a rotary microtome.

*Staining sequences.* Imprints were stained with Wright's/Giemsa technique to permit analysis of general cell morphology. Hematoxylin and eosin was used to stain

representative sections to permit analysis of general tissue morphology. Additional imprints and tissue sections were stained at room temperature using a modification of Perls' (Prussian blue) technique (20) to visualize non-heme ferric iron (19). Tissue sections were deparaffinized in sequential xylene/alcohol baths before staining. In brief, imprint and tissue section slides were 1) hydrated in distilled water; 2) placed in potassium ferrocyanide/hydrochloric acid working solution for 10 minutes; 3) rinsed in distilled water, counterstained in nuclear fast red for 5 minutes, and washed in running tap water for 2 minutes; and 4) dehydrated and cleared with 95% ethyl alcohol, absolute ethyl alcohol, and xylene for two changes each for 2 minutes each (19, 21). Appropriate positive and negative control slides were prepared and examined with each staining run. Each slide was reviewed simultaneously by both authors using a double-headed binocular light microscope at 100X - 400X and graded for AFR as described below.

**Evaluation and Grading Of Macrophage Acid Ferrocyanide Reactivity (AFR).** *Definition of Macrophage and Macrophage AFR.* Macrophages were defined as large phagocytic mononuclear cells usually (but not invariably) found in locations other than the blood (22 - 24). Morphologically, these cells typically appear with a non-segmented, often slightly indented nucleus which is eccentrically situated in the cytoplasm. The cytoplasm is often punctuated with multiple vacuoles or phagocytosed particulate matter, especially brownish pigment(s), and may exhibit pseudopod-like projections (22 - 24 ). Within the kidneys, spleens, and livers of most teleosts, macrophages occur prominently in well-circumscribed, membrane-bound pigmented nodules (melanomacrophage centers, MMC) (4, 25, 26). Other macrophages may occur as peri-arterial accumulations (ellipsoids) or as scattered, isolated cells in these organs (26 - 28). The AFR in fish macrophages consists largely or entirely of iron-laden ferritin or partially degraded ferritin in the form of hemosiderin (4, 8, 10, 24). Other hematopoietic cells were also identified using standard morphologic criteria (22 - 24).

*Imprint Preparations.* Imprints were considered evaluable if a variety of hematopoietic cells were present, if most cells were intact, and if macrophages could be readily identified. Evaluable kidney imprints were required to contain one or more renal tubules. Grading was performed in areas of slides where there was a monolayer of cells with adequate cell separation. These criteria were used to assign a semi-quantitative histochemical grade (AFRG) to each imprint preparation: grade 0 - no detectable AFR; 1 - AFR rarely detected (< 1 positive macrophage per field at 400X); cytoplasmic AFR usually faint blue-gray blush; grade 2 - AFR occasionally detected (1 - 5 AFR-positive macrophages per field at 400X); cytoplasmic reactivity usually faint blue or finely granular; grade 3 - AFR readily apparent (5 - 10 AFR-positive macrophages per field at 400X); cytoplasmic reactivity usually finely granular or sometimes coarsely granular; and grade 4 - AFR marked (> 10 AFR-positive macrophages per field at 400X); cytoplasmic reactivity usually coarsely granular (often blue-black). Extracellular or artefactual AFR was not graded. Twelve replicate cytologic preparations were randomly prepared and selected from all specimens to evaluate consistency of AFRG values.

*Tissue Sections.* Sections were considered evaluable if cellular morphology were intact, and if focal accumulations of macrophages (MMC) or scattered macrophages could be identified readily. These criteria were used to assign a semi-quantitative macrophage AFRG to each slide preparation: grade 0 - no detectable AFR in MMC; 1 - AFR in < 25% of MMC; cytoplasmic reactivity usually faint blue-gray blush, or involves few macrophages in MMC; grade 2 - AFR in 25 - 50% of MMC; cytoplasmic reactivity usually faint blue-gray blush or finely granular, or involves approximately one-third of macrophages in MMC; grade 3 - AFR in 50 - 75% of MMC; cytoplasmic reactivity usually finely granular or sometimes coarsely granular, or involves approximately two-thirds of macrophages in MMC; and grade 4 - AFR in > 75% of MMC; cytoplasmic reactivity usually coarsely granular (often blue-black) or involves most macrophages in MMC. AFR in ellipsoids and scattered macrophages was similarly graded. Extracellular

or artefactual AFR was not included in determining the AFRG. The appearance of pigment in macrophages was reported as yellow, yellow-brown, brown, or black, as previously described (29).

**Comparison of AFRG Values in Imprint and Tissue Section Preparations.** Values of AFRG in imprint and tissue section preparations in kidneys of a bonito, an amberjack, a gag, and a gray triggerfish, and in the spleens of a cobia and a gray triggerfish were compared.

**Correlation of AFRG in Kidney and Spleen Imprint Preparations.** In the channel catfish, paired kidney and spleen imprints from six individuals were evaluated. We also computed the correlation of paired kidney and spleen AFRG in 13 individuals of six families (blue runner, black grouper, gag, rock sand perch, bank sea bass, speckled hind, lane snapper, vermillion snapper, red porgy, whitebone porgy, blackfin tuna, false albacore, and tomtate).

**AFRG in Kidney and Spleen Imprints of Fish Grouped by Taxonomic Family:** Macrophage AFRG in the kidneys and spleens of diverse species of teleosts were tabulated according to taxonomic families. These were unpaired specimens obtained from individuals other than those used for paired kidney and spleen AFRG analysis (see above).

**Statistical Considerations:**

Numbers of specimens in categories were enumerated by direct counting. Kidney and spleen macrophage AFRG obtained using imprint preparations were expressed as mean ± 1 S.D.; values were rounded to the nearest tenth for presentation. The correlation coefficient *r* was computed to compare the values of macrophage AFRG in replicate imprint slides, to compare the values of AFRG in corresponding imprint and tissue section preparations, and to compare the mean kidney and spleen macrophage AFRG in

individual species. Statistics were computed using GB-STAT v. 6.5 (Dynamic Microsystems, Inc., Silver Spring, MD). A value of $p < 0.05$ was defined as statistically significant.

**Results:**

**General Evaluation of Kidney and Spleen Preparations**: *Imprint Preparations:* MMC and scattered macrophages were present in imprints of kidney or spleen from most species, although many MMC appeared to be partially disrupted. Erythroid cells were the predominant hematopoietic cell type observed in all preparations. AFR was not detected in non-macrophage cells, although the occurrence of small or faint deposits of AFR which would have required > 400X magnification for detection cannot be excluded. There was a significant positive correlation of the respective AFRG in 12 pairs of replicate slides of 5 kidney and 7 spleen preparations representing 9 species and 6 taxonomic families ($r = 0.6623$; $p = 0.02$).

*Tissue Sections:* Individuals of five species were studied. MMC were observed in sections of kidney or spleen from each, although the appearance of the MMC varied widely. Erythroid cells were the predominant hematopoietic cell type observed in all preparations. In the kidney of a false albacore (*Euthynnus alletteratus* Rafinesque), the renal tubules appeared small; hematopoietic cells which occupied the intertubular spaces represented much of the bulk of the organ. Many pigment-laden macrophages were scattered in the hematopoietic tissue. There were many large MMC characterized by a thick peripheral membrane, dense black pigment, and moderate AFR; in many MMC, the AFR was greater around the periphery of the MMC. Macrophages scattered in the intertubular areas also contained moderate AFR consistent with hemosiderin (AFRG 2). In the spleen of a cobia (*Rachycentron canadum* Linnaeus), MMC were small, relatively sparsely distributed within the organ, and contained yellow-black pigment and trace AFR

(AFRG 1). In the kidney of a greater amberjack (*Seriola dumerili* Risso), MMC were medium in size, moderately frequent, contained black pigment, and had no AFR (AFRG 0). Additional pigment was observed within the lumen of blood vessels. In the kidney of a gag *(Mycteroperca microlepis* Goode and Bean), MMC were small, moderately frequent, contained black pigment, and had no AFR (AFRG 0). In the kidney of a gray triggerfish (*Ballistes capriscus* Gmelin), the renal tubules were the predominant structures in the organ; MMC were small, sparsely distributed, contained yellow-black pigment, and had no AFR (AFRG 0). In the spleen of the same triggerfish, MMC were small to medium in size, sparsely distributed, contained yellow pigment, and had moderate AFR consistent with hemosiderin (AFRG 2). Outside MMC, yellow-brown pigment was observed in macrophages in areas of erythroid cells. AFR was not observed in splenic peri-arterial macrophages (ellipsoids) in any species studied. AFR was not detected in non-macrophage cells, although the occurrence of small or faint deposits of AFR which would have required > 400X magnification for detection cannot be excluded. AFR was not identified in erythroid cells, granulocytes, or thrombocytes.

There was greater differentiation of staining in cell types and subcellular structures in kidney and spleen specimens fixed in buffered formol acetone and subsequently stained with hematoxylin and eosin. For AF staining of sections, neutral buffered formalin fixation gave slightly improved differentiation of general morphology than buffered formol acetone in some sections. However, the appearance of AFR was similar in all sections regardless of the fixative used.

**Comparison of AFRG Values in Imprint and Tissue Section Preparations.** Values of AFRG in paired imprint and tissue section preparations of the four kidneys and two spleens of five species, each of a different taxonomic family. There was a significant positive correlation of these six pairs of values ($r = 0.9518$; $p = 0.003$).

**AFRG in Kidney and Spleen Imprint Preparations of Fish Grouped by Taxonomic Family:** Macrophage AFR consistent with hemosiderin was detected in many but not all species (Table 1). In three species (blue runner, speckled hind, and gag), AFR was not detected in kidney or spleen. In seven other species (blackfin tuna, false albacore, bank sea bass, vermillion snapper, red porgy, whitebone porgy, and tomtate), AFR was typically detected in both organs (Table 1). Macrophage AFR was not observed in either organ in the channel catfish (Ictaluridae) or in several species of the Carangidae (Table 1). In the Serranidae, Lutjanidae, and Sparidae, intermediate mean values of AFRG were obtained in both organs. Somewhat greater mean values of AFRG were obtained in fish of the families Scombridae, Ballistidae, and Pomadasyidae (Table 1).

**Correlation of AFRG in Kidney and Spleen Imprint Preparations.** In the channel catfish, paired kidney and spleen imprints from six individuals were examined, and there was no AFR in any specimen (Table 1). We computed the correlation of kidney and spleen AFRG in 13 individuals in which both organs of the same individual were studied; this represented one each of 13 marine species of six taxonomic families. Overall, the kidney AFRG values ranged from 0 to 4, and the spleen AFRG values ranged from 0 to 3. Across the 13 species, the correlation coefficient of respective mean kidney and spleen AFRG values was not significant ($r = 0.4194$; $p = 0.15$). A comparison of mean AFRG values of fish grouped by taxonomic families suggests that spleen AFR is greater than kidney AFR, on the average (Table 1).

**Discussion:**

Semi-quantification of macrophage iron using AF-stained organ imprints and the present grading criteria provide a simple, replicable, and inexpensive method by which relative quantities of non-heme ferric iron in kidneys or spleens of bony fish can be estimated and compared. Using this approach, AFR in kidneys and spleens of teleost fishes observed

by light microscopy is localized in macrophages, consistent with the present and past results obtained with analysis of tissue sections (13, 17). We did not study teleost fishes such as salmonids which possess scattered macrophages in hematopoietic organs but lack MMC (29). However, our results in species in which AF-reactive macrophages occurred in MMC and were also scattered within the renal red pulp and the renal intertubular hematopoietic tissue, *e.g.*, false albacore, suggest that the present method of semi-quantification of macrophage-associated ferric iron is applicable to the study of fishes without MMC. Our study was limited to species of relatively large fishes from which organ imprints could be made readily by hand. Analysis of specimens from smaller species or from immature fish could require a modified approach to making and grading organ imprints or smears. Interference of ceroid or other pigment in teleost MMC centers with the interpretation of AF staining has been reported frequently in tissue sections of teleost spleens (6, 30, 31). Because the preparation of imprints partially disrupts MMC, imprints may be less sensitive to this interference than tissue sections.

The present use of specific grading criteria and numerical grades permits statistical analysis of results, in contrast to a non-quantitative grading method using paraffin sections (8, 10, 13, 28). The present method may be less precise than one in which the area of AFR in tissue sections is quantified using video image capture and computerized measurement of microscopic images (17). However, the present method does not require tissue sections or computerized equipment, and thus may be more adaptable to clinical and field studies in which rapidly available, inexpensive estimates of organ iron content may be desirable. Neither the present semi-quantitative results nor those previously reported (13, 17) have been compared directly to kidney or spleen iron content measured with a quantitative method such as atomic absorption spectrometry.

In healthy teleost fishes, studies using AF staining (4, 8 - 10, 13, 31 - 33) and radioiron (3) demonstrate that splenic macrophages of the MMC and red pulp readily phagocytose

mature, effete, or heterologous erythrocytes more readily than do renal macrophages. Accordingly, the spleen iron content of many species is greater than that of kidney when histochemical, radioisotopic, or biochemical methods of analysis are used (3, 6, 13). In the present study, we also observed that spleen macrophage AFRG was generally greater than that in the kidney among fish grouped by taxonomic families, confirming previous observations (13). The present results also demonstrate that there may not be a precise correlation between values of AFRG in kidney and spleen in the same individual, a conclusion suggested by previous data (10, 13). Taken together, however, these observations suggest that the spleen may act as an important site of iron storage.

Radioisotope studies indicate that iron from defective juvenile erythrocytes produced in the kidney (ineffective or inefficient erythropoiesis) is readily recycled (3, 34). This supports the postulate that the kidney macrophage iron pool is more labile than that of the spleen. This is consistent with histologic observations in the rainbow trout (*Salmo gairdneri* Richardson) that kidney macrophages can phagocytose erythrocytes *in vitro* (7), but the kidney macrophages almost always lack AFR *in vivo* (12, 13). Taken together, these observations suggest that much iron released by kidney macrophages may be transported to maturing erythroid cells for hemoglobin synthesis and that the iron subsequently leaves the kidney via mature erythrocytes (3, 35).

Disordered iron metabolism in teleost fishes may be evaluable by the present histochemical and grading techniques. Iron deficiency induced by bleeding can reduce kidney and spleen iron content significantly (6). Hemolysis due to acetylphenylhydrazine administration (33), infections (9, 13), vitamin E deficiency (36), starvation (13), or exposure to crude petroleum or other industrial contaminants (17, 37 - 39) is associated with increased AFR in spleen macrophages. In contrast, AFR in the kidney and liver may remain low under these conditions (13). Experimentally-induced iron overload in fish increases AFR in hematopoietic organs and can also cause hemolysis

(41, 42). Finally, alterations in kidney or spleen AFR may be more readily discerned in species which normally possess little or no AFR in these organs, *e.g.,* the channel catfish or certain members of the family Carangidae.

**Acknowledgements:**

Channel catfish were made available through the courtesies of Farm Fresh Catfish, Inc., Greensboro, AL. The authors appreciate the cooperation and assistance of Captain Eric Williams, Mr. and Mrs. Roy Martin, Mrs. Kathy Ward, and numerous licensed sport fishermen in Destin, Florida in obtaining specimens from marine fish. Ms. Suzan Smith of Cunningham Pathology Associates, P.C. of Birmingham, Alabama provided general advice about histotechnique and acid ferrocyanide staining.

## References

1. Klaverkamp JF, Turner MA, Harrison SSE, Hesslein RH. Fates of metal radiotracers added to a whole lake: accumulation in slimy sculpin (*Cottus cognatus*) and white sucker (*Catastomus commersoni*). Sci Total Environ 1983;28:119-128.

2. Carpene E, Serra R, Manera M, Isani G. Seasonal changes of zinc, copper, and iron in gilthead sea brean (*Sparus aurata*) fed fortified diets. Biol Trace Elem Res 1999; 69:121-139.

3. Hevesy G, Lockner D, Sletten K. Iron metabolism and erythrocyte formation in fish. Acta Physiol Scand 1964;60:256-266.

4. Agius C. The melano-macrophage centres of fish: a review. Fish Immunol 1985; 24:85-105.

5. Baptist JP, Hoss DE, Lewis CW. Retention of $^{51}Cr$, $^{60}Co$, $^{65}Zn$, $^{85}Sr$, $^{95}Nb$, $^{141m}In$, and $^{131}I$ by the Atlantic croaker (*Micropogon undulatus*). Health Phys 1970;18:141-148.

6. Walker RL, Fromm PO. Metabolism of iron by normal and iron deficient rainbow trout. Comp Biochem Physiol 1976;55A:311-318.

7. Braun-Nesje R, Bertheussen K, Kaplan G, Seljelid R, Salmonid macrophages: separation, *in vitro* culture and characterization. J Fish Dis 1981;4:141-151.

8. Fulop GM, McMillan DB. Phagocytosis in the spleen of the sunfish *Lepomis* spp. J Morphol 1984;179:175-195.

9. Falk K, Press CM, Landsverk T, Dannevig BH. Spleen and kidney of Atlantic salmon (*Salmo salar* L.) show histochemical changes early in the course of experimentally induced infectious salmon anaemia (ISA). Vet Immunol Immunopathol 1995;49:115-126.

10. Tokumaru M, Ferri AG. Histochemistry of the pigments found in the liver, spleen and kidney of the fresh-water fish. Brasil Biol Rev 1970;30:163-171.

11. Ellis AE. Leukocytes and related cells in the plaice *Pleuronectes platessa.* J Fish Biol 1976;8:143-156.

12. Oguri M. Histochemical observation on the dark brown pigment granules in the kidney tissue of rainbow trout. Bull Jap Soc Sci Fish 1976;42:1223-1227.

13. Agius C. The role of melano-macrophage centres in iron storage in normal and diseased fish. J Fish Dis 1979;2:337-343.

14. Kato T, Shinjo S, Shimada T. Isolation and properties of ferritin from tuna fish (Thunnus obesus) spleen. J Biochem (Tokyo) 1968;63:170-175.

15. Suryakala S, Deshpande V. Purification and characterization of liver ferritins from different animal species. Vet Res Commun 1999;23:165-181. J Biochem (Tokyo) 1968;63:170-175.

16. Geetha C, Deshpande V. Purification and characterization of fish liver ferritins. Comp Biochem Physiol B Biochem Mol Biol 1999;123:285-294.

17. Khan RA, Nag K. Estimation of hemosiderosis in seabirds and fish exposed to petroleum. Bull Environ Contam Toxicol 1993;50:125-131.

18. Hoese HD, Moore RH. Fishes of the Gulf of Mexico. Texas, Louisiana, and adjacent waters. College Station, Texas A & M University Press, 1977; 327 pages.

19. Barton JC, Parmley RT, Butler TW, Williamson SE, Lilly MB, Gualtieri RJ, Heck LW Jr: Differential staining of neutrophils and monocytes: surface and cytoplasmic iron-binding proteins. Histochem J 1988;20:147-155.

20. Perls M. Nachweis von Eisenoxyd in gewissen Pigmenten. Arch Pathol Anat [Virchow] 1867;39:42-48.

21. Parmley RT, Barton JC. Cytochemistry of blood and marrow cells. *In* Histochemistry in Pathologic Diagnosis (Spicer SS, ed.). New York: Marcel Dekker, Inc, 1987;127-178.

22. Williams RW, Warner MC. Some observations of the stained blood cellular elements of channel catfish, *Ictalurus punctatus*. J Fish Biol 1976;9:491-487.

23. Ellis AE. The leucocytes of fish: a review. J Fish Biol 1977;11:453-491.

24. Rowley AF, Hunt TC, Page M, Mainwaring G. Fish. *In* Vertebrate blood cells (Rowley AF, Ratcliffe NA, eds.). Cambridge, Cambridge University Press, 1988; pp. 19-128.

25. Roberts RJ. Melanin-containing cells of teleost fish and their relation to disease. *In* The pathology of fishes (Ribelin WE, Migaki G, eds), University of Wisconsin Press, Madison, 1976; 399-428.

26. Ellis AE, Munroe ALS, Roberts RJ. Defence mechanisms in fish. I. A study of the phagocytic system and the fate of intraperitoneally injected particulate material in the plaice (*Pleuronectes platessa* L.). J Fish Biol 1976;8:67-78.

27. Fänge R, Nilsson S. The fish spleen: structure and function. Experientia 1985; 41:152-158.

28. Ferguson HW. The relationship between ellipsoids and melano-macrophage centres in the spleen of turbot (*Scophthalmus maximus*). J Comp Path 1976;86:377-380.

29. Agius C. Phylogenetic development of melano-macrophage centres in fish. J Zool Lond 1980;191:11-31.

30. Wood EM, Yasutake WT. Ceroid in fish. Am J Pathol 1956;32:591-603.

31. Grover JH. Hemosiderin in bluegill spleens. Trans Am Fish Soc 1968;97:48-50.

32. Agius C, Agbede SA. An electron microscopical study on the genesis of lipofuscin, melanin, and haemosiderin in haemopoietic tissues of fish. J Fish Biol 1984;24:471-488.

33. Herraez MP, Zapata AG. Structure and function of the melano-macrophage centres of the goldfish *Carassius auratus*. Vet Immunol Immunopathol 1986;12:117-126.

34. Topf W. Über die Blutbildung und die Blutbildungsstätten beim Karpfen. Zool Anz 1953;150:91-104.

35. Yu M L, Kiley CW, Sarot DA, Permutter A. Relation of hemosiderin to erythropoiesis in the blue gourami, *Trichogaster tricopterus*. J Fish Res Bd Can 1971; 28:47-48.

36. Wilson RP, Bowser PR, Poe WE. Dietary vitamin E requirement of fingerling channel catfish. J Nutr 1984;114:2053-2058.

37. Haensly WE, Neff JM, Sharp JR, MorrisAC, Bedgood MF, Beom PD. Histopathology of *Pleuronectes platessa* L. from Aber Wrac'h and Aber Be Benoit, Brittany, France: long-term effects of the Amoco Cadiz crude oil spill. J Fish Dis 1982;5:365-391.

38. Khan RA, Kiceniuk JW. Histopathological effects of crude oil on Atlantic cod following chronic exposure. Can J Zool 1984;62:2038-2043.

39. Khan RA. Effect of oil-contaminated sediment on the longhorn sculpin (*Myoxocephalus octodecemspinosus*) following chronic exposure. Bull Environ Contam Toxicol 1991;47:63-69.

40. Khan RA, Hooper RG. Decontamination of winter flounder (*Pleuronectes americanus*) following chronic exposure to effluent from a pulp and paper mill. Arch Environ Contam Toxicol 2000;38:197-201.

41. Cheung PJ, Nigrelli RF, Ruggieri GD, Gold K, Baiardi JC. Fish as models for hemosiderosis. Ann N Y Acad Sci 1980;344:336-351.

42. Standal H, Rorvik KA, Lien H, Andersen O. Effects of acute iron overload on Atlantic salmon (*Salmo salar*) and rainbow trout (*Oncorhynchus mykiss*). Biol Trace Elem Res 1997;59:13-22.

**Table 1.** Macrophage Acid Ferrocyanide Reactivity Grades (AFRG) in Kidneys and Spleens of Teleost Fishes.*

| Family | Number of Species (*n*) | Kidney AFRG (*n*) | Spleen AFRG (*n*) |
|---|---|---|---|
| | | | |
| Ictaluridae | 1 (6) | 0.0 ± 0.0 (6) | 0.0 ± 0.0 (6) |
| Carangidae | 3 (9) | 0.0 ± 0.0 (2) | 0.0 ± 0.0 (7) |
| Serranidae | 6 (17) | 0.1 ± 0.4 (7) | 1.2 ± 1.3 (10) |
| Lutjanidae | 3 (11) | 0.6 ± 0.8 (7) | 0.9 ± 1.1 (4) |
| Sparidae | 3 (6) | 1.0 ± 0.0 (3) | 1.0 ± 1.0 (3) |
| Scombridae | 3 (2) | 2.8 ± 0.5 (5) | 2.0 ± 1.2 (4) |
| Ballistidae | 1 (7) | 0 (1) | 2.0 ± 1.3 (7) |
| Pomadasyidae | 2 (5) | 4 (1) | 2.5 ± 1.3 (4) |

* These AFRG were derived from imprint preparations; data are expressed as mean ± 1 S.D. (*n*). Kidney and spleen values of AFGR were derived from paired specimens in the six channel catfish; the remaining data were derived from unpaired specimens. These fishes were identified as Ictaluridae: channel catfish (*Ictalurus punctatus* Rafinesque) (6); Carangidae: greater amberjack (*Seriola dumerili* Risso) (5), blue runner (*Caranx fusus* Geoffroy Saint-Hilaire) (3), and crevalle (*Caranx hippos* Linnaeus) (1); Serranidae: bank sea bass (*Centropristis ocyura* Jordan and Evermann) (5), gag (*Mycteroperca microlepis* Goode and Bean) (4), sand perch (*Diplectrum formosum* Linnaeus) (3), black grouper (*Mycteroperca bonaci* Poey) (2), speckled hind (*Epinephelus drummondhayi* Goode and Bean) (2), and warsaw (*Epinephelus nigritus* Holbrook) (1); Lutjanidae: lane snapper (*Lutjanus synagris* Linnaeus) (4), vermillion snapper (*Rhomboplites aurorubens* Cuvier) (4), and red snapper (*Lutjanus campechanus* Poey) (3); Sparidae: red porgy (*Pagrus sedecim* Ginsburg) (3), whitebone porgy (*Calamus leucosteus* Jordan and Gilbert) (2), and

pinfish (*Lagodon rhomboides* Linnaeus) (1); Scombridae: black-fin tuna (*Thunnus atlanticus* Lesson) (4), false albacore (*Euthynnus alletteratus* Rafinesque) (4), and king mackerel (*Scomberomorus cavalla* Cuvier) (1); Ballistidae: gray triggerfish (*Ballistes capriscus* Gmelin) (7); and Pomadasyidae: tomtate (*Haemulon aurolineatum* Cuvier) (4), and pigfish (*Orthopristis chrysoptera* Linnaeus) (1).

## Ellen Barton Biography

Ellen Barton is a native of Birmingham, Alabama and will graduate in the Rhodes College class of 2002. She is a Biology and French double major and plans to study in France in the summer of 2001. She has special interests in medicine and research. As part of her second year studies at Rhodes, she participated in an internship at the Veterans Affairs Medical Center in Memphis, Tennessee. In the summer of 1999, she worked with her father Dr. Barton and other collaborators at Southern Iron Disorders Center, Birmingham, Alabama, and earned authorship on a paper about the treatment of iron deficiency with intravenous iron dextran which was published in *The American Journal of Medicine.* In the summer of 2000, she worked in the laboratory of Dr. Ronald T. Acton, Director of the Immunogenetics Program, University of Alabama at Birmingham, Birmingham, Alabama. As a first author reporting this research, she described the prevalence of a newly-discovered alternate transferrin receptor mutation in Caucasians and African Americans with and without hemochromatosis and iron overload in *Blood Cells, Molecules, and Diseases*. Ellen is a member of Beta Beta Beta Biology Honor Society, a member of Kappa Delta sorority, and a volunteer at Youth Villages.